UNIVERSITY OF TURKU

QUANTUM INFORMATION PROTOCOLS AND THERMODYNAMICS WITH OPEN QUANTUM SYSTEMS

Sina Hamedani Raja

TURUN YLIOPISTON JULKAISUJA – ANNALES UNIVERSITATIS TURKUENSIS
SARJA – SER. AI OSA – TOM. 636 | ASTRONOMICA – CHEMICA – PHYSICA – MATHEMATICA | TURKU 2020

UNIVERSITY OF TURKU

QUANTUM INFORMATION PROTOCOLS AND THERMODYNAMICS WITH OPEN QUANTUM SYSTEMS

Sina Hamedani Raja

TURUN YLIOPISTON JULKAISUJA – ANNALES UNIVERSITATIS TURKUENSIS
SARJA – SER. AI OSA – TOM. 636 | ASTRONOMICA – CHEMICA – PHYSICA – MATHEMATIC | TURKU 2020

University of Turku

Faculty of Science and Engineering
Department of Physics and Astronomy
Laboratory of Theoretical Physics
Doctoral programme in Physical and Chemical Sciences

Supervised by

Sabrina Maniscalco
Department of Physics and Astronomy
University of Turku
Finland

Jyrki Piilo
Department of Physics and Astronomy
University of Turku
Finland

Reviewed by

Steve Campbell
School of Physics
University College Dublin
Ireland

Nadja K. Bernardes
Departamento de Fisica
Universidade Federal de Pernambuco
Brazil

Opponent

Gabriele De Chiara
School of Mathematics and Physics
Queen's University Belfast
UK

The originality of this publication has been checked in accordance with the University of Turku quality assurance system using the Turnitin OriginalityCheck service.

ISBN 978-951-29-8275-2 (PRINT)
ISBN 978-951-29-8276-9 (PDF)
ISSN 0082-7002 (Print)
ISSN 2343-3175 (Online)
Painosalama Oy, Turku, Finland 2020

Acknowledgements

You found me right now, behind these words. This is me...traveling through the *unknown*. Not sure where I was, where I am, where to head. I just know the beauty of each route I walked, the beauty of understanding a tiny part of the unknown...the beauty of sharing what I know. Without you finding me, I was just wandering through the unknown.

You found me at the start of a long journey, my doctoral studies. Sabrina and Jyrki, you taught me the art of traveling and you were the biggest support and true inspiration during this journey. Sabrina, thank you for believing in me, for your continuous support and for your excellent leadership. Jyrki, thanks for countless times I enjoyed discussing physics with you, and thanks for your amazing supervision.

You found me at the end of this journey. I would like to thank Dr. Steve Campbell and Dr. Nadja K. Bernardes for pre-examining the thesis and I warmly thank the opponent of my doctoral dissertation, Dr. Gabriele De Chiara.

You found me in between. Nicola, a special thanks to you for all your wise advises and the nice project we had together. Thank you Elsi, Massimo, Göktuğ and Rebecca for advising my first doctoral research works. I would like to thank you Teiko for your great lectures and your unique sense of humor. Henri, I am grateful to you for all the moments we discussed physics or laughed together to the worst jokes, even during the toughest days! Zhao-Di, you are a true magician in the lab, I am honored to work with you. Thank you people of the corridor, from the silent room to the noisy room, you are all amazing friends. My ex-roommates, Antti, Johannes and Jakko, I enjoyed every minute of sharing the office with you. My dear current roommates, Laura, Boris and Oskari, I truly enjoyed keeping the silent room noisy with you during these years! I am also grateful to all my dear friends outside of work. The joyful times we spent together helped me cope with the difficulties during this journey. I always felt home thanks to you all.

You found me at the start of everything. My dearests, Mother, father, you are the first beauties in my life and the brightest ones. Your sincere devotion to me can not be replaced with anything. Mother, thanks for teaching me responsibility and discipline, for showing me how to live and love. Father, thanks for teaching me resilience and hard working, you introduced science to me and you were my first inspiration to follow this path. My dear sisters, Sahar and Haleh, you are two angels in my life. I am always thankful for your unconditional devotion to me. Dear parents-in-law, I could not start this journey without your support, love and encouragement. I could not start the biggest journey of my life without you letting me into your warm family, my family. Mehran, Alireza, Pouya, Kian and Koosha, having you in my life has gave me the power to handle the biggest challenges. My beloved Mamani, you kept calling me "Dr." till it came true! I am honored that you always believed in me. You have been always the compass in my life.

I found you, and you found me! Pegah, my love, my true friend, and my great inspiration. I was able to complete this journey only because of your unconditional support and encouragement. Your love has made the biggest challenges easy to me. This is now us...traveling through the unknown together.

You have walked all the paths I wish to walk. You have seen all the beauty I wish to see. Dedicated to you, who know all the unknown...to Rostin and Shakiba.

Contents

Abstract

The theory of open quantum systems deals with the inevitable interaction between a quantum system of interest and its surrounding environment, the resulting non-unitary dynamics of the system and its decoherence. On the one hand, the interaction with the environment is a challenge for quantum technologies that aim to provide fast and secure quantum computation and communication. On the other hand, the open system dynamics is a natural framework to study thermodynamics of quantum systems, concerning both fundamental aspects and applications such as miniaturized thermodynamic machines. In this thesis, we utilize open quantum systems both to perform quantum information protocols and to study the relation between dynamical and thermodynamic properties of the quantum systems under scrutiny.

After a brief review of some essential concepts of quantum theory, the results of the original articles are summarized. The results are grouped into two parts. The first part focuses on quantum information protocols with open systems. Unlike the conventional approaches, here we actually use the environment to perform the task of the protocols. The central tool in this part is the non-local memory effects implemented by the two-photon dephasing model. A master equation approach to this model is presented which adds to the previous results based on the dynamical map point of view. We then employ the non-local memory effects as a resource to remotely generate polarization entanglement induced by interference in the frequency degrees of freedom and also to experimentally realize a high-fidelity quantum teleportation protocol with open systems.

The relation between the dynamics and the thermodynamics of the quantum systems is explored in the second part of the thesis. A controllable model for the transition from Markovian to non-Markovian dynamics of a qubit is presented. We derived the corresponding master equation to capture the reduced dynamics of the qubit and found that non-Markovianity suppresses the ability to perform work on it. Finally, the finite-time driving

effects on the performance of a quantum Stirling heat engine is explored. We found a direct relation between the performance of the heat engine and the different time scales involved in the dynamics of the driven working substance. In particular, a simultaneous efficiency and power boost is discussed and the effect of asymmetric driving protocols for expansion and compression processes is addressed.

Tiivistelmä

Avoimien kvanttisysteemien teoria käsittelee kiinnostuksen kohteena olevan kvanttisysteemin vuorovaikutusta ympäristönsä kanssa. Vuorovaikutuksesta seuraavaa systeemin epäunitaarista aikakehitystä ja koherenssien katoamista, dekoherenssia. Ympäristön kanssa tapahtuva vuorovaikutus on haaste kvanttiteknologioille, joiden tarkoituksena on tarjota nopeaa kvanttilaskentaa ja turvallista kommunikointia. Toisaalta, avoimen systeemin aikakehitys on luonnollinen viitekehys tutkia kvanttisysteemien termodynamiikkaa, käsitellen sekä perustavanlaatuisia näkökohtia että käytännön sovelluksia, kuten miniatyyrimaisia termodynaamisia koneita. Tässä väitöskirjassa avoimia kvanttisysteemejä hyödynnetään sekä kvantti-informaatioprotokollien toteutuksessa että kvanttisysteemin aikakehitykseen liittyvien ja termodynaamisten ominaisuuksien välisen suhteen tutkimiseen.

Kvanttimekaniikan oleellisimpien käsitteiden lyhyen kertauksen jälkeen esitetään väitöstyön alkuperäisten julkaisujen tulosten yhteenveto. Tulokset on ryhmitelty kahteen osaan: Ensimmäinen osa keskittyy avoimilla systeemeillä toteutettaviin kvantti-informaatioprotokolliin. Toisin kuin tavanomaisessa lähestymistavassa, tässä ympäristöä hyödynnetään protokollan tavoitteen toteutumisessa. Tämän osan keskeinen työkalu ovat epälokaalit muisti-ilmiöt toteutettuna kahden fotonin dephasing-melussa. Ensimmäisessä osassa esitellään master-yhtälöön perustuva lähestymistapa tähän melutyyppiin, mikä tuo lisäarvoa aikaisempiin tuloksiin, jotka perustuvat dynaamisiin karttoihin. Sitten hyödynnämme epälokaaleja muisti-ilmiöitä resurssina etänä tapahtuvassa polarisaatiokietoutumisen generoinnissa toteutettuna taajuusvapausasteiden interferenssillä sekä korkean fideliteetin kvanttiteleportaation kokeellisessa toteutuksessa avoimilla kvanttisysteemeillä.

Väitöskirjan jälkimmäisessä osassa tutkitaan kvanttisysteemin aikakehityksen ja termodynamiikan suhdetta. Esitämme mallin, jossa kubitin aikakehityksen muutosta Markovisesta epä-Markoviseksi voidaan hallita. Johdimme vastaavan master-yhtälön ratkaistaksemme kubitin redusoidun

aikakehityksen ja selvitimme, että epä-Markovisuus estää tekemästä kubittiin työtä. Viimeisenä tutkitaan äärellisessä ajassa tehtävän systeemin ajon vaikutusta kvantti-Stirling-lämpövoimakoneen suorituskykyyn. Löysimme suoran yhteyden lämpövoimakoneen suorituskyvyn ja työtä tekevän aineen aikaskaalojen välillä. Erityisesti käsitellään samanaikaista hyötysuhteen ja tehon parannusta sekä epäsymmetristen ajoprotokollien käyttöä laajenemis- ja kompressioprosesseissa.

List of papers

This thesis consists of a review of the subject and the following original research articles:

I **Remote polarization-entanglement generation by local dephasing and frequency up-conversion**,
S. Hamedani Raja, G. Karpat, E.-M. Laine, S. Maniscalco, J. Piilo, C.-F. Li, G.-C Guo, Phys. Rev. A **96**, 013844 (2017).

II **Thermodynamic fingerprints of non-Markovianity in a system of coupled superconducting qubits**,
S. Hamedani Raja, M. Borrelli, R. Schmidt, J. P. Pekola, S. Maniscalco, Phys. Rev. A **97**, 032133 (2018).

III **Photonic dephasing dynamics and the role of initial correlations**,
S. Hamedani Raja, K. P. Athulya, A. Shaji, J. Piilo, Phys. Rev. A **101**, 042127 (2020).

IV **Experimental realization of high-fidelity teleportation via non-Markovian open quantum system**,
Z.-D. Liu, Y. N. Sun, B.-H. Liu, C.-F. Li, G.-C. Guo, *S. Hamedani Raja*, H. Lyyra, J. Piilo, arXiv:2007.01318 (2020).

V **Finite-time quantum Stirling cycle**,
S. Hamedani Raja, S. Maniscalco, J. P. Pekola, G.-S. Paraoanu, N. Lo Gullo, arXiv:2009.10038 (2020).

Other published material

This is a list of the publications produced which have not been chosen as a part of this doctoral thesis

- **Entanglement protection via periodic environment resetting in continuous-time quantum-dynamical processes**,
  T. Bullock, F. Cosco, M. Haddara, *S. Hamedani Raja*, O. Kerppo, L. Leppäjärvi, O. Siltanen, N. W. Talarico, A. De Pasquale, V. Giovannetti, S. Maniscalco, Phys. Rev. A **98**, 042301 (2018).

Chapter 1

Introduction

Quantum theory is a probabilistic theory describing the stochastic nature of the universe at very small scales. In the quantum world, a particle can simultaneously follow in two different paths – behaving like a wave – until one observes its location. Yet incompatible measurements can not be performed accurately at a single experimental arrangement. The experimentalist needs to decide which behavior of the quantum object she wants to observe, i.e, its wave or particle behavior. Bohr denoted this complementary principle an *elementary quantum phenomenon*. Miller and Wheeler illustrated this phenomenon as a smoky dragon whose tail and head correspond respectively to experimental arrangement and outcome of the experiment, whereas, the body of the dragon in between is smoky and undefined to us [1, 2]. Despite its departure from our everyday life, predictions of quantum theory have been realized with high accuracy in the experimental tests. Many new possibilities have emerged that were out of imagination in classical physics. This also led quantum mechanics to become intertwined with different fields of physics, providing fundamental insights and technological advancements. In particular, quantum information theory and quantum thermodynamics have been of high importance.

The basic unit of information in a quantum system is called the *qubit*. The quantum superposition principle makes qubits fundamentally different to classical bits. Utilizing quantum superposition allows quantum algorithms to outperform classical counterparts [3–11]. In addition, the superposition principle in multipartite quantum systems leads to pure quantum correlation [12], named *entanglement* by Schrödinger [13]. Quantum entanglement is a resource in quantum information processing, enabling teleportation of an unknown quantum state [14, 15], quantum superdence coding [16, 17], and quantum secure key distribution [18–20]. Simulation

of physical systems on quantum devices is the other important aspect of the quantum world [21, 22], especially when it comes to the tasks that can not be simulated on a classical computer [23]. Thanks to recent technological advancements, we live in the era of *Noisy Intermediate-Scale Quantum* (NISQ) technologies [24]. Nowadays, *quantum supremacy* is claimed to be realized on an actual quantum device [25], ground to satellite quantum teleportation [26] and intercontinental quantum key distribution [27] are implemented, and small scale quantum computers are available to public by companies like IBM [28].

Despite all of these breakthroughs, we are still far from realizing large scale fault tolerant quantum computers. This is mostly due the fact that quantum systems are very prone to the noise induced by their interaction with the surrounding environment. As perfect isolation of a system is out of reach, all quantum systems are inevitably open to interact with their surroundings. The system-environment interaction, also known as open system dynamics, destroys coherence and entanglement of the system in a process named *decoherence* [29–31]. Therefore, any quantum information processing task has to be done on a time scale smaller than the decoherence time of the qubits. These facts have attracted a lot of attention to the theory of open quantum systems, aiming to first understand and then tackle decoherence. For example, addressing memory effects in the dynamics of open systems have attracted much attention both theoretically and experimentally [32–36]. Lots of effort have been also done to minimize the effects of decoherence via, for example, dynamical decoupling, decoherence-free subsystems, and error-correction [37, 38].

The other interdisciplinary field in quantum theory deals with thermodynamic properties of the quantum systems. From the birth of quantum mechanics it has been a challenge to revisit the laws of thermodynamics, governing the macroscopic world close to equilibrium, by starting from the quantum realm, which deals with microscopic systems at finite sizes and usually out of equilibrium. These challenges engendered the rise of the so-called quantum thermodynamics. Thanks to recent advances in experimental design and control of quantum systems and also to new theoretical and numerical tools, quantum thermodynamics has received much attention during the last two decades. There are a vast number of open questions covered in the field, as it is listed in the recent book [39]. For example, *what is the right definition of process-dependent quantities like work and heat in the quantum realm? How does equilibration of a quantum system*

arise from quantum properties? Are quantum thermal machines superior to their classical counterparts due to the presence of coherence and entanglement? Also many different research topics exist, for example, thermoelectricity [40], resource theory of thermodynamics [41], information-theoretic approaches [39], and quantum fluctuation relations [39, 42].

A powerful tool in quantum thermodynamics is the the theory of open quantum systems [39, 43, 44]. The concept of an open system – with factorized initial condition – provides a natural partitioning of the system and the heat bath, which is required in thermodynamics. Once the separation of the system and the bath is established, one can study flow of energy and entropy between the two parts as well as generation of entropy in the system and bath. Emergence of thermodynamic laws from quantum mechanics can be consistently formulated by semi-group Markovian dynamics [39, 43], which is a pillar of the theory of open quantum systems. Thermodynamics in a non-Markovian situation is also investigated for example in Refs [45, 46]. Open system dynamics also allows for studying and implementing quantum counterparts of the classical heat engines, where a single quantum system plays the role of the working substance [39, 47, 48].

This thesis is developed around new results in the theory of open quantum systems with direct applications in quantum information theory and quantum thermodynamics. The structure of the thesis is the following. In Chapter 2, we review the basics of quantum theory and present an introduction to the concepts in quantum information theory and quantum thermodynamics that have been used in deriving the results of the thesis. The main results of the thesis are accordingly divided in two parts, presented in Chapter 3 and Chapter 4.

Chapter 3 is devoted to the quantum information protocols with open quantum systems. Central to the results of this part is the concept of non-local memory effects induced by initial correlations in the state of the environment [49, 50]. A controllable experimental platform to implement non-local memory effects is the two-photon dephasing model [51]. The main objective of this part of the thesis has been to develop quantum information protocols with open quantum systems enhanced by non-local memory effects. Utilization of non-local memory effects to enhance a protocol with noisy systems has been considered previously for example in superdense coding [52]. Before presenting the protocols, we first shed some light on the two-photon dephasing dynamics by deriving a master equation. Although this dynamics has been studied earlier using the dynamical map

approach [49, 50], a master equation point of view was missing. In Article III, we derive such a master equation and discuss the effects of initial correlations of the environment on the decay rates and operatorial form of the master equation. In Article I, we present a protocol for generating polarization entanglement remotely. By utilizing non-local memory effects in the two-photon dephasing model, we discuss how local photonic dephasing and local frequency upconversion can be employed to generate entanglement between two distant photons. Interestingly, this protocol can be described by an interferometric approach, where overlapping paths of an interferometer allow for interference-induced generation of entanglement. In Article IV, we experimentally realized the protocol to perform high-fidelity teleportation with open quantum systems. The original idea has been introduced in [53], where the authors have shown how the two-photon dephasing model and non-local memory effects allow for perfect teleportation despite the presence of local noise. To make an experimental realization possible, we have modified the protocol by encoding the Alice's state on the spatial degrees of freedom of her photon, instead of using the polarization degrees of freedom of a third photon.

Chapter 4 is then dedicated to the discussion of the open system dynamics as a tool in quantum thermodynamics. In Article II, we introduce a simple model based on two interacting qubits for implementing a controllable non-Markovian dynamics. We derive a master equation for this model and discuss its validity concerning different physical parameters involved in the dynamics. Using this master equation, we study the Markovian to non-Markovian transition of the model by manipulating the qubit-qubit interaction strength. Once the open dynamics is obtained, we examine it to find a possible link between the extent of non-Markovianity of the dynamics and the ability of an external drive to perform work on the system. Article V is more involved with the thermodynamic ideas and is concentrated on the study of a quantum thermodynamic cycle running at finite times. Implementing thermodynamic machines that convert heat to work faces a dilemma: efficiency of the machine is the highest when it is operating in a quasistatic regime, at which the output power vanishes. We introduce a model and analyze the open system dynamics of a driven qubit as the working substance in a quantum Stirling cycle used as a heat engine. To study the dynamics we derive a non-Markovian master equation without any assumption on the separation of the time scales of the drive and the qubit. Then the performance of the cycle, with regards to efficiency and

power, is discussed in details considering different time scales of the drive and the role of asymmetric driving speeds.

Finally, Chapter 5 concludes the results of the thesis and presents the possible outlooks of the work.

Chapter 2

Quantum systems

In this chapter, we recall the basic concepts and tools used in developing the results of the thesis. In the first section, some basic elements of the quantum theory are reviewed. Then we present the theoretical descriptions for the dynamics of closed and open quantum systems in section 2. We proceed to recall some selected concepts in quantum information theory and quantum thermodynamics, respectively in section 3 and section 4.

2.1 Basics of quantum theory

In a physical theory we map physical concepts onto a mathematical language according to some correspondence rules. For instance, momentum of an object in classical mechanics is a physical concept that we map onto a set of real numbers. In quantum theory, however, mathematical formalism is not so trivial as we cannot predict the exact value of a physical concept, but rather only the probability of observing a specific value is available. Moreover, unlike classical mechanics, where physical concepts usually take a continuous spectrum, quantum quantities are often *quantized*, as the word quantum suggests. Experiments in quantum physics usually consist of three parts: *state preparation*, *evolution*, and *measurement*. In the state preparation phase, the experimenter prepares an ensemble of identically prepared systems which determines a well-defined probability distribution for all given observables to be measured. The mathematical formalism of quantum theory describing all the steps is based on the tools of *linear algebra* and *probability theory* [54–56].

Quantum states live in *Hilbert space*, denoted by $\mathcal{H}$, defined as the complex linear space of the vectors with finite norm with respect to their

inner product. We indicate with d the dimension of the Hilbert space, which gives the maximum number of linearly independent and orthogonal vectors in the space. The set of normalized orthogonal vectors, denoted by $\{|\phi_i\rangle\}_{i=1}^{d}$, provides a complete basis for the vector space such that any vector $|\psi\rangle \in \mathcal{H}$ can be written as $|\psi\rangle = \sum_i c_i |\phi_i\rangle$. The space of quantum states is a linear operator space ($\mathcal{L}$) of the self-adjoint non-negative and trace class operators with trace 1 acting on $\mathcal{H}$, i.e., $\mathcal{S}(\mathcal{H}) = \{\rho \in \mathcal{L}(\mathcal{H}) | \rho^\dagger = \rho,\ \rho \geq 0,\ \mathrm{tr}[\rho] = 1\}$. Non-negativity and trace 1 restrictions on the states guarantee a well-defined probability distribution. States ρ are usually called *density matrices* and are divided into two classes of *pure* and *mixed* states. A pure state cannot be written as a nontrivial convex combination of other states and is of the form $\rho = |\psi\rangle\langle\psi|$, whereas a mixed state can be written as $\rho = \sum_i p_i \rho_i$, where $\sum_i p_i = 1$ and $\rho_i \in \mathcal{S}(\mathcal{H})$. To take care of multipartite quantum systems, we need to consider the tensor product of the Hilbert spaces of each party. For example, considering system A and system B we have $\rho_{AB} \in \mathcal{S}(\mathcal{H}_{AB})$ with $\mathcal{H}_{AB} := \mathcal{H}_A \otimes \mathcal{H}_B$. One of the distinct features of quantum mechanics is that there can exist density matrices on the multipartite spaces, say on the bipartite space $\mathcal{S}(\mathcal{H}_{AB})$, such that a decomposition of the form $\rho_{AB} = \sum_i p_i \rho_i^A \otimes \rho_i^B$ with $\rho^{A(B)} \in \mathcal{S}(\mathcal{H}_{A(B)})$ does not exist. This class of quantum states have a quantum type of correlation named *entanglement*. On the other hand, if a state can be written as the tensor product of reduced states, we call it a *factorized* state which does not possess any entanglement.

For each physical observable in quantum theory there is assigned a Hermitian operator on $\mathcal{L}(\mathcal{H})$. Assume for example a variable named r which takes a discrete set of possible values $\{r_i\}$. Let's call the corresponding operator to the variable r by R. Then for a given density matrix ρ, the averaged value (expectation value) of the operator R is given by $\langle \mathrm{R} \rangle_\rho := \mathrm{tr}[\rho \mathrm{R}]$. If we assume the spectral decomposition $R = \sum_i r_i |r_i\rangle\langle r_i|$ with $r_i \in \mathbb{R}$, the averaged value will be given by $\langle \mathrm{R} \rangle_\rho := \sum_i r_i \mathrm{tr}[\rho |r_i\rangle\langle r_i|] = \sum_i r_i p_i$, where p_i is the probability of obtaining an outcome r_i. The general mathematical formalism describing a measurement is given by the so-called *positive operator valued measures* (POVM). In this formalism, for the set of possible outcomes $\{e_i\}$ one assigns a set of positive operators $\{\mathrm{E}_i\}$ on $\mathcal{L}(\mathcal{H})$, such that $\sum_i \mathrm{E}_i = \mathrm{I}$ and the probability of each outcome e_i is given by $p_i = \mathrm{tr}[\rho \mathrm{E}_i]$.

2.2 Dynamics of quantum systems

2.2.1 Closed systems

Time evolution of a closed quantum system – a system that is isolated from the rest of the universe – denoted by the state vector $|\psi(t)\rangle \in \mathcal{H}$ is given by the Schrödinger equation ($\hbar = 1$)

$$i\frac{d}{dt}|\psi(t)\rangle = \mathrm{H}(t)\,|\psi(t)\rangle\,, \tag{2.1}$$

where $\mathrm{H}(t)$ is the Hamiltonian of the quantum system. The solution of the Schrödinger equation gives a unitary operator which maps the initial state at time t_0 to a final legitimate state at time t, such that

$$|\psi(t)\rangle = \mathrm{U}(t,t_0)\,|\psi(t_0)\rangle\,,\quad \mathrm{U}(t,t_0) = \mathcal{T}e^{-i\int_{t_0}^{t} d\tau \mathrm{H}(\tau)}. \tag{2.2}$$

Here $\mathcal{T}$ denotes the time-ordering operator in case the Hamiltonian does not commute with itself at different times, i.e., $[\mathrm{H}(t_2),\mathrm{H}(t_1)] \neq 0$ for $t_2 \neq t_1$, where $[\mathrm{A},\mathrm{B}] := \mathrm{AB} - \mathrm{BA}$. Also note that $\mathrm{U}(t_i,t_i) = \mathrm{I}$. Time evolution of a pure state can be generalized to any mixed state $\rho(t_0) = \sum_j p_j\,|\psi_j(t_0)\rangle\,\langle\psi_j(t_0)|$, such that

$$\rho(t) = \mathrm{U}(t,t_0)\rho(t_0)\mathrm{U}(t,t_0)^\dagger =: \mathcal{U}(t,t_0)[\rho(t_0)], \tag{2.3}$$

where, $\mathcal{U}[\cdot]$ is a *superoperator* acting on the operators on $\mathcal{S}(\mathcal{H})$, and plays the same role as the unitary operator in Eq. (2.2) for the density matrices. If we take derivative of Eq. (2.3) with respect to t, we get

$$\frac{d}{dt}\rho(t) = -i[\mathrm{H}(t),\rho(t)], \tag{2.4}$$

which is the equivalent of Schrödinger equation for a general mixed state and is called Liouville-von Neumann equation.

2.2.2 Open Systems

The notion of a closed system presumes perfect isolation of the system under scrutiny. Fulfilling this condition is often out of reach, urging us to deal with open systems which inevitably interact with their surrounding

environments. Suppose that we are interested in the dynamics of a quantum system labeled by S. However, the system S interacts with its surrounding environment denoted by E, which may incorporate the rest of the universe. Despite of the size the environment E may have, the combined system $S + E$ is closed and its dynamics is given by the Schrödinger equation. However, at the end of the day we are only interested in the system S, and hopefully not the whole universe, so we need to derive the reduced dynamics of system S by starting from the dynamics of the combined system $S + E$. Let us introduce the dynamical map $\Phi_t[\cdot]$ which maps the initial density matrix ρ_0 to a final one at time $t > 0$, such that $\rho(t) = \Phi_t[\rho(0)]$. To guarantee physicality of the reduced dynamics, the dynamical map must meet *completely positivity* (CP) and *trace preserving* (TP) requirements. The CP condition means that for all $\rho \in \mathcal{S}(\mathcal{H}_S \otimes \mathcal{H}_{dim(k)})$ and any $k \in \mathbb{N}^+$, we have $(\Phi_t \otimes \mathrm{I}_k)[\rho] \geq 0$. The TP condition requires that trace of the density matrix does not change upon the action of the map, i.e., $\mathrm{tr}[\Phi_t[\rho]] = \mathrm{tr}[\rho]$ for all $\rho \in \mathcal{S}(\mathcal{H}_S)$. Moreover, the dynamical map is independent of the input state and depends solely on the properties of the environment E and its coupling to the open system.

Factorized initial state of the extended quantum system $S + E$, i.e., $\rho_{SE}(0) = \rho_S(0) \otimes \rho_E(0)$, is necessary for completely positivity of the map [31]. Assume the factorized initial condition and let us set the initial time to zero, i.e., $t_0 = 0$. We consider the unitary evolution of the system $S + E$ corresponding to the total Hamiltonian of the combined system, denoted by H_{SE}, and then take the partial trace with respect to the system E to get

$$\rho_S(t) = \mathrm{tr}_E\big[\mathrm{U}(t,0)\rho_S(0) \otimes \rho_E(0)\mathrm{U}(t,0)^\dagger\big]. \tag{2.5}$$

It can be shown that if the state of the environment is fixed, Eq. (2.5) can be written as

$$\rho_S(t) = \sum_i \mathrm{K}_i(t)\rho_S(0)\mathrm{K}_i(t)^\dagger, \tag{2.6}$$

where $\sum_i \mathrm{K}_i(t)^\dagger \mathrm{K}_i(t) = \mathrm{I}$. The form given in Eq. (2.6) is called *Kraus representation*. Strictly speaking, a dynamical map is CP if and only if it has a Kraus representation [57].

Let us discuss in more detail how to derive the reduced dynamics of the system S. Consider the state of the combined system denoted by $\rho_{SE}(t)$.

Our aim is to find an equation of motion (the so-called *master equation*) for the reduced state $\rho_S(t) = \mathrm{tr}_E[\rho_{SE}(t)]$. One should start by using Eq. (2.4) with regards to the total system $S + E$, thus

$$\frac{d}{dt}\mathrm{tr}_E[\rho_{SE}(t)] = -i\mathrm{tr}_E[\mathrm{H}_{SE}, \rho_{SE}(t)], \tag{2.7}$$

where H_{SE} is the total Hamiltonian of the system $S + E$, including the interaction between the two subsystems. A well-known procedure to proceed from the equation above and derive a master equation is provided by the *Nakajima-Zwanzig* method [29, 31]. Considering two orthogonal projection operators $\mathcal{P}$ and $\mathcal{Q} = \mathrm{I} - \mathcal{P}$, with $\mathcal{P}\rho_{SE} = \mathrm{tr}_E[\rho_{SE}] \otimes \rho_E$, this method follows formal steps to obtain an equation of motion for $\mathcal{P}\rho_{SE}$. Assuming the factorized initial condition $\rho_{SE}(0) = \rho_S(0) \otimes \rho_E(0)$ and a stationary environment, one gets an equation of motion for $\rho_S(t)$ given by an integro-differential equation of the form

$$\frac{d}{dt}\rho_S(t) = \int_0^t d\tau \mathcal{K}(t,\tau)\rho_S(\tau). \tag{2.8}$$

Here $\mathcal{K}(t,\tau)$ is the *memory kernel*, meaning that the instantaneous evolution of the reduced state at time t depends on a memory of the evolution at previous times $\tau \leq t$. A wide class of physical models deals with weak-coupling limit and non-structured environments. In that situation, applying further assumptions such as the Born and Markov approximations relaxes the dependency of the evolution on its past memory. It is usually possible to transform the master equation in Eq. (2.8) into a time-convolutionless form [29, 31, 58]

$$\frac{d}{dt}\rho_S(t) = \mathcal{L}(t)[\rho_S(t)], \tag{2.9}$$

where $\mathcal{L}(t)$ is a superoperator acting on the state of the open system at time t. Actually, $\mathcal{L}(t)$ is the generator of the dynamics, such that one obtains the dynamical map $\Phi_t[\cdot]$ formally by

$$\Phi_t := \mathcal{T}\exp[\int_0^t \mathcal{L}(\tau)d\tau]. \tag{2.10}$$

Physicality constraint of the dynamical map Φ_t naturally puts some restrictions on the generator $\mathcal{L}(t)$. The simplest case is when the generator

is time-independent and the dynamics is memory-less, thus $\Phi_t = \exp[t\mathcal{L}]$. A consequence of this simple form is that $\Phi_{t_2}\Phi_{t_1} = \Phi_{t_1+t_2}$, which gives a semigroup of dynamical maps. This is not a group due to the lack of a CP inverse of the dynamical maps. The generator $\mathcal{L}$ corresponds to a CP semigroup dynamical map if and only if it has the so-called Lindblad form [59, 60]

$$\mathcal{L}[\rho_S(t)] = -i[\mathrm{H}_S, \rho_S(t)] + \sum_i \gamma_i \big[\mathrm{A}_i \rho(t) \mathrm{A}_i^\dagger - \frac{1}{2}\{\mathrm{A}_i^\dagger \mathrm{A}_i, \rho(t)\}\big], \qquad (2.11)$$

where $\{\mathrm{X}, \mathrm{Y}\} = \mathrm{XY} + \mathrm{YX}$. Here operators A_i, which act on $\mathcal{S}(\mathcal{H}_S)$, are the Lindblad operators and $\gamma_i \in \mathbb{R}^+$ are some constant transition rates. The master equation above can be generalized to include time-dependent rates and Lindblad operators, such that

$$\mathcal{L}(t)[\rho_S(t)] = -i[\mathrm{H}_S, \rho_S(t)] + \sum_i \gamma_i(t) \big[\mathrm{A}_i(t) \rho(t) \mathrm{A}_i^\dagger(t) - \frac{1}{2}\{\mathrm{A}_i^\dagger(t)\mathrm{A}_i(t), \rho(t)\}\big], \qquad (2.12)$$

with $\gamma_i(t) \in \mathbb{R}^+$ [31]. If the rates in Eq. (2.12) take temporal negative values, some extra conditions must be fulfilled to guarantee complete positivity of the map, for example see [61, 62].

Non-Markovian dynamics

Consider that the master equation in Eq. (2.12) is in the *canonical* form, i.e. $\mathrm{tr}\left[\mathrm{A}_i^\dagger(t)\mathrm{A}_j(t)\right] = \delta_{ij}$, $\mathrm{tr}\left[\mathrm{A}_i(t)\right] = 0$, and H_S is Hermitian; then the generated dynamics is *Markovian* (memory-less) if and only if the decay rates $\gamma_i(t)$ be positive [63]. Strictly speaking, defining quantum Markov processes is not as straightforward as in the classical realm due to disturbing nature of the quantum measurement, which affects the posterior statistics [32]. A common definition of a quantum Markov process is based on the CP *divisibility* of the dynamical maps [64, 65]. Any CP dynamical map Φ_t can be decomposed as $\Phi_t = \Lambda(t, s)\Phi_s$ for any $0 \leq s \leq t$, where $\Lambda(t, s)$ is a propagator of the dynamics from time s to time t. A dynamical map is CP-divisible (Markovian) if the propagator $\Lambda(t, s)$ is also CP for all $s \in [0, t]$. If it is not, the dynamics is non-Markovian. To witness non-Markovianity of a dynamical map one takes an information measure which contracts with

the CP maps [32, 33], for instance trace distance [66], volume of accessible states [67], or quantum channel capacity [68]. Consequently, any temporal increase of that measure indicates violation of CP divisibility, meaning the dynamics is non-Markovian with respect to that measure.

For the sake of simplicity of the calculations in Article II, we have specifically used the volume of accessible states as a witness of non-Markovianity [67]. This is, however, just a witness of non-Markovianity as it may fail to detect non-divisibility of the dynamical map. Nonetheless, non-Markovianity detected by this approach always implies non-divisibility as well as backflow of information [69]. Assume an N-level quantum system with a density matrix $\rho(t) \in \mathcal{S}(\mathcal{H}_N)$. Assume $\{\mathrm{G}_i\}_{i=0}^{N^2-1}$ as the set of all normalized generators of $SU(N)$ plus the normalized identity operator $\mathrm{G}_0 = \mathbb{I}_N/\sqrt{N}$. Since this set provides a complete operator basis on $\mathcal{S}(\mathcal{H}_N)$, the density matrix of the system can be decomposed as

$$\rho(t) = \sum_{i=0}^{N^2-1} r_i(t)\mathrm{G}_i, \tag{2.13}$$

where $r_i = \mathrm{tr}[\mathrm{G}_i\rho]$ denotes the coordinates of a generalized Bloch vector $\vec{r}(t) = (r_0(t), r_1(t), ...)^T$. Applying the same decomposition for the evolved state $\rho(t) = \Phi_t[\rho(0)]$, with CPTP dynamical map Φ_t, gives an affine transformation of the generalized Bloch vector given by

$$\vec{r}(t) = \mathbf{F}(t)\vec{r}(0), \tag{2.14}$$

where $\mathbf{F}(t)$ is a $N^2 \times N^2$ matrix corresponding to the map Φ_t. Providing a geometric description for the density matrix by the generalized Bloch vector allows us to assign a volume $V(t)$ for the accessible states during the evolution. This volume has a relation $d^N V(t) = \|\mathbf{F}_t\| d^N V(0)$, where $\|\cdot\|$ denotes determinant. Since $\|\mathbf{F}_t\|$ is a contracting function of time for a CPTP dynamical map, any temporal increase in $\|\mathbf{F}_t\|$ corresponds to non-Markovianity. Therefore, the authors of Ref [67] introduced a measure of non-Markovianity given by

$$\mathcal{N} = \int_{\partial_t\|\mathbf{F}_t\|>0} \partial_t\|\mathbf{F}_t\|. \tag{2.15}$$

2.3 Information of quantum systems

2.3.1 Coherence and entanglement

In this subsection, we briefly review the concepts of quantum coherence and entanglement. These peculiar properties of quantum systems, once challenging our understanding about local-reality [12], turned to be the most prestigious resources for developing quantum algorithms that do not have a classical counterpart [5, 7, 8, 14, 16, 18–20].

Quantum coherence

Linearity of the Hilbert space means that if two states $|\psi_1\rangle$ and $|\psi_2\rangle$ are valid state vectors on the Hilbert space $\mathcal{H}$, then according to the *superposition principle* any linear combination of them, e.g., $|\psi_3\rangle = \alpha\,|\psi_1\rangle + \beta\,|\psi_2\rangle$ with $|\alpha|^2 + |\beta|^2 = 1$, is also a legitimate state vector on $\mathcal{H}$. The coherent superposition of the two vectors is fundamentally different to a classical ensemble of the states and leads to striking consequences like *quantum interference*. Consider the density matrix $\rho = |\psi_3\rangle\langle\psi_3|$, therefore the expectation value of an observable A is given by

$$\langle\psi_3|\,\mathrm{A}\,|\psi_3\rangle = |\alpha|^2\,\langle\psi_1|\,\mathrm{A}\,|\psi_1\rangle + |\beta|^2\,\langle\psi_2|\,\mathrm{A}\,|\psi_2\rangle + 2\mathrm{Re}[\alpha\beta^*\,\langle\psi_1|\,\mathrm{A}\,|\psi_2\rangle], \tag{2.16}$$

where $\mathrm{Re}[\cdot]$ denotes the real part. The first two terms on the r.h.s of Eq. (2.16) is the classical sum of the expectation values of observable A w.r.t. the states $|\psi_1\rangle$ and $|\psi_2\rangle$ and a probability distribution $\{|\alpha|^2, |\beta|^2\}$. The last term, however, does not have any classical counterpart and corresponds to the interference of the two states involved in the superposition. Note that a state vector can be written as a coherent superposition of vector basis, i.e., $|\psi\rangle = \sum_i c_i\,|\phi_i\rangle$, thus the corresponding density matrix has the form $\rho = \sum_{i,j} c_i c_j^*\,|\phi_i\rangle\langle\phi_j|$. In this regard, coherence is related to the off-diagonal elements of the density matrix denoted by $\rho_{ij} := \langle\phi_i|\,\rho\,|\phi_j\rangle$ with $i \neq j$. Recently, a resource theory of quantum coherence (RTQC) has been introduced which provides a systematic way to define a proper measure of quantum coherence [70]. The two widely used functions that fulfill RTQC requirements are *relative entropy of coherence* and l_1*-norm*. The latter is

defined by

$$C_{l_1}(\rho) := \sum_{i \neq j} |\rho_{ij}|, \tag{2.17}$$

and will be used in this thesis as a measure of quantum coherence due to its simple form.

Quantum Entanglement

An interesting consequence of quantum superposition which reveals itself when considering multipartite systems is quantum entanglement. Assume, for example, a bipartite system with Hilbert space $\mathcal{H}_{AB} = \mathcal{H}_A \otimes \mathcal{H}_B$. As mentioned earlier, an entangled state on $\mathcal{S}(\mathcal{H}_{AB})$ is unfactorizable, i.e., $\rho_{AB} \neq \sum_i p_i \rho_i^A \otimes \rho_i^B$ with $\rho^{A(B)} \in \mathcal{S}(\mathcal{H}_{A(B)})$. Considering the local vector basis of a two-qubit system denoted by $\{|0\rangle, |1\rangle\}$, one can check that the state vector $|\Psi^+\rangle = (|0\rangle|1\rangle + |1\rangle|0\rangle)/\sqrt{2}$ is indeed entangled.

When there is non-zero entanglement between the parties of a bipartite pure state $|\psi\rangle$, the reduced state obtained by $\rho_{A(B)} = \mathrm{tr}_{B(A)}[\rho_{AB}]$ will be mixed. This fact reflects itself to define *entropy of entanglement* as a measure of entanglement [71]. Entropy of entanglement of a pure bipartite state $|\psi\rangle$ is defined by [1]

$$E(|\psi\rangle) := -\mathrm{tr}(\rho_{A(B)} \log(\rho_{A(B)})). \tag{2.18}$$

Furthermore, for a general bipartite mixed state written as an ensemble of pure states, namely $\rho_{AB} = \sum_i p_i |\psi_i\rangle\langle\psi_i|$, *entanglement of formation* is defined as the least expected entanglement of such an ensemble [71, 72], such that

$$E(\rho_{AB}) = \min_{\{p_i, |\psi_i\rangle\}} [\sum_i p_i E(|\psi_i\rangle)]. \tag{2.19}$$

A systematic way to define proper measures of entanglement is characterized by resource theory of quantum entanglement (RTQE) [73, 74]. According to RTQE, a so-called entanglement monotone maps all separable (non-entangled) states to zero and should be non-decreasing upon *local operations and classical communications* (LOCC). The latter means that by

[1] Not to be mistaken with the notation previously used for denoting an environment.

applying a CPTP map on a local qubit of a two-qubit entangled state the entanglement of the bipartite state never increases. Entanglement of formation is one of such monotones that fulfills these requirements. Although handling the optimization in Eq. (2.19) is difficult in general, a compact analytic form is available for two-qubit mixed states using *concurrence* [72]. For a given two-qubit state ρ one defines

$$\tilde{\rho} = (\sigma_y \otimes \sigma_y)\rho^*(\sigma_y \otimes \sigma_y), \tag{2.20}$$

where σ_y is the second Pauli operator. Then concurrence of the state ρ is obtained by

$$\mathcal{C}(\rho) = \max\{0, \lambda_1 - \lambda_2 - \lambda_3 - \lambda_4\}, \tag{2.21}$$

where λ_i are the eigenvalues of the non-Hermitian matrix $\rho\tilde{\rho}$ in decreasing order. Having the concurrence, one calculates the entanglement of formation by $E(\rho) = \mathcal{E}(C(\rho))$, where

$$\mathcal{E}(\mathcal{C}) = h(\frac{1+\sqrt{1-\mathcal{C}^2}}{2}), \tag{2.22}$$

and $h(x) = -x\log x - (1-x)\log(1-x)$.

2.3.2 Coherence and entanglement in an interferometric setup

Wave-particle duality is one of the most peculiar aspects of quantum mechanics. In a given experimental setup, a quantum object shows either its wave or particle behavior by *a priori* adapting to that setup. In this section, we briefly review the concept of wave-particle duality in a quantum information context, namely duality relation between coherence and which-path information. After that, we show how erasing the available information revives the coherence and allows for the interference to happen.

Coherence versus which-path information

Assume a particle entering a generalized N-port interferometer, in a superposed state

$$|\psi\rangle = \sum_{i}^{N} \sqrt{p_i}\,|i\rangle\,, \tag{2.23}$$

where each $|i\rangle$ denotes a port of interferometer and $\sum_i p_i = 1$. Let the particle inside the interferometer interact with a detector which is initially in the state $|d_0\rangle$ available to all the ports. Consider now that the interaction, governed by a unitary evolution, maps the initial state of the detector to a final state that corresponds to the port that the particle has occupied, namely $\mathrm{U}(|i\rangle\,|d_0\rangle) = |i\rangle\,|d_i\rangle$. This means that after the interaction with the detector, the state of the particle plus the detector is evolved to a potentially entangled state given by

$$|\xi\rangle = \sum_{i}^{N} \sqrt{p_i}\,|i\rangle\,|d_i\rangle\,. \tag{2.24}$$

The reduced state of the particle, after tracing over the detector's degrees of freedom, reads

$$\rho = \sum_{i,j=1}^{N} \sqrt{p_i p_j}\langle d_j|d_i\rangle\,|i\rangle\,\langle j|\,. \tag{2.25}$$

The question is now how the particle's coherence has evolved due to the interaction with the detector? Using the l_1-norm as the measure of coherence, the particle's state had an initial coherence

$$C_{l_1}(|\psi\rangle\,\langle\psi|) = \sum_{i\neq j} \sqrt{p_i p_j}, \tag{2.26}$$

whereas, after interacting with the detector its coherence has changed to

$$C_{l_1}(\rho) = \sum_{i\neq j} \sqrt{p_i p_j}|\langle d_j|d_i\rangle|. \tag{2.27}$$

The extent to which coherence of the system has changed depends on the overlap of the detector vectors $|d_i\rangle$, so the amount of *which-path infor-*

mation available by measuring the detector's state. Considering the most informative scenario where $\langle d_i|\, d_j\rangle = \delta_{ij}$, we realize that the system's state has been evolved to a diagonal one with zero coherence. In this case, one gains complete information about the path of the particle by performing a measurement on the state of the detector which discriminates between the vectors $|d_i\rangle$.

There are different ways to quantify the information a detector carries about the particle's state (its path inside an interferometer), e.g., unambiguous state discrimination [75] or minimum-error state discrimination method [76]. For a given measure of coherence denoted by C and a given measure of path information denoted by P there holds an inequality relation of the form

$$C^2 + P^2 \leq X^2, \tag{2.28}$$

where X is some finite constant. Consequently, there is always a trade-off between coherence and path information; the more path information is available, the less coherence is present in the system. We stress that the discussion mentioned here is quite general and is not model-dependent. In other words, for any physical model with an N-dimensional Hilbert space $\mathcal{H}_N$, a given vector basis spanning $\mathcal{H}_N$ can play the role of an N-port interferometer.

Erasing the which-path information

What happens if we somehow discard the available which-path information? Assume a two-level system on a Hilbert space spanned by the vector basis $\{|0\rangle, |1\rangle\}$. Starting from a given state $|\psi\rangle = \alpha\,|1\rangle + \beta\,|0\rangle$ let the system interact with another two-level system, playing the role of a detector with the orthogonal pointer vectors $\{|0\rangle_d, |1\rangle_d\}$, to reach a correlated state

$$|\Psi\rangle = \alpha\,|1\rangle\,|1\rangle_d + \beta\,|0\rangle\,|0\rangle_d\,. \tag{2.29}$$

Due to the correlation between the two systems the reduced state of the system is mixed, $\rho = |\alpha|^2\,|1\rangle\langle 1| + |\beta|^2\,|0\rangle\langle 0|$. Now consider a vector basis of the detector Hilbert space that includes superposition of the old basis, namely $|\pm\rangle = (|1\rangle_d \pm |0\rangle_d)/\sqrt{2}$. Writing the total state in the new basis

yields

$$|\Psi\rangle = \frac{1}{\sqrt{2}}\left[(\alpha\,|1\rangle + \beta\,|0\rangle)\,|+\rangle + (\alpha\,|1\rangle - \beta\,|0\rangle)\,|-\rangle\right]. \tag{2.30}$$

Consider a selective measurement with the projector $P_+ = |+\rangle\langle+|$. The outcome will be

$$\frac{P_+\,|\Psi\rangle}{\mathrm{tr}[\langle\Psi|\,P_+\,|\Psi\rangle]} = |\psi\rangle\,|+\rangle\,, \tag{2.31}$$

which is a factorized state and does not possess any which-path information. The aforementioned procedure is a simple example of a *quantum eraser*. Quantum erasure can be performed in different ways [77–80], but the common feature of all procedures is erasing the correlation between the system's degrees of freedom and other degrees of freedom in order to discard the available which-path information. Here, we introduced an eraser based on selective measurement on the detector degrees of freedom, similar to the method used in [80].

2.3.3 Quantum Teleportation

Quantum teleportation of an unknown state is a quantum algorithm based on local operations and classical communication which relies on entanglement as the resource. Here we briefly review the standard teleportation protocol [14]. Assume that Alice and Bob share an entangled two-qubit system in the state $|\Phi^+\rangle_{23} = (|00\rangle_{23} + |11\rangle_{23})/\sqrt{2}$. Alice possesses a state $|\phi\rangle_1 = \alpha\,|0\rangle_1 + \beta\,|1\rangle_1$ that she wants to teleport to Bob. Therefore, the total state of the three qubits (two of Alice labeled by $1, 2$ and one of Bob labeled by 3) reads

$$|\Xi\rangle_{123} = \frac{1}{\sqrt{2}}\,|\phi\rangle_1\,(|00\rangle_{23} + |11\rangle_{23}). \tag{2.32}$$

Consider now the entangled basis on Alice's two-qubit system given by

$$|\Phi^{\pm}\rangle_{12} = \frac{1}{\sqrt{2}}(|00\rangle_{12} \pm |11\rangle_{12}), \quad |\Psi^{\pm}\rangle_{12} = \frac{1}{\sqrt{2}}(|01\rangle_{12} \pm |10\rangle_{12}). \tag{2.33}$$

Rewriting the state in Eq. (2.32) with regards to the so-called *Bell basis* of Alice defined above results in

$$\begin{aligned}|\Xi\rangle_{123} = \frac{1}{2}\Big[&|\Phi^+\rangle_{12}(\alpha|0\rangle_3 + \beta|1\rangle_3) + |\Phi^-\rangle_{12}(\alpha|0\rangle_3 - \beta|1\rangle_3) \\ &+ |\Psi^+\rangle_{12}(\alpha|1\rangle_3 + \beta|0\rangle_3) + |\Psi^-\rangle_{12}(\alpha|1\rangle_3 - \beta|0\rangle_3)\Big].\end{aligned} \tag{2.34}$$

At this point Alice performs a measurement on her two-qubit system considering the Bell basis in Eq. (2.33). Suppose the outcome of her measurement is the Bell state $|\Phi^-\rangle$, thereby Alice knows that the state of Bob's qubit has collapsed to $|\phi\rangle_3 = \alpha|0\rangle_3 - \beta|1\rangle_3$. However, if Bob does not know the result of the measurement, he has to trace over the two qubits of Alice to get his reduced state. This gives him a mixed state (due to the correlation between Alice and Bob). Nonetheless, if Alice shares her result with Bob using a classical communication line, Bob realizes that his state is $|\phi\rangle_3$. Having this state, Bob only needs to apply a σ_z rotation on his qubit to fulfill a high fidelity teleportation. Note that if Alice's outcome was $|\Phi^+\rangle, |\Psi^+\rangle, |\Psi^-\rangle$, Bob can complete the protocol by applying local unitaries $\mathrm{I}, \sigma_x, i\sigma_y$ on his qubit, respectively.

2.4 Thermodynamics of quantum systems

2.4.1 An open system point of view

The theory of open quantum system naturally describes the quantum thermodynamic framework since it starts from partitioning the total system into the system of interest and its surrounding environment [43]. Once separation of the systems is established, we can define thermodynamic quantities within each subsystem and their flow. Assume a quantum system interacting with an external large system, namely a heat bath. The total state of the system and the bath is denoted by $\rho_{tot}(t) \in \mathcal{S}(\mathcal{H})$, with $\mathcal{H} = \mathcal{H}_S \otimes \mathcal{H}_B$. The total Hamiltonian of the composite system reads

$$\mathrm{H}(t) = \mathrm{H}_S(t) + \mathrm{H}_B + \mathrm{H}_I, \tag{2.35}$$

where $\mathrm{H}_S(t)$ is a time-dependent Hamiltonian for the system, H_B is the Hamiltonian of the bath and H_I is the interaction Hamiltonian between

the two. The evolution of the total system is unitary and is given by

$$\rho_{tot}(t) = \mathrm{U}(t)\rho_{tot}(0)\mathrm{U}(t)^\dagger, \quad \mathrm{U}(t) = \mathcal{T}e^{-i\int_0^t d\tau \mathrm{H}(\tau)}. \tag{2.36}$$

In general we are interested in the reduced dynamics and thermodynamics of the system S. To have a legitimate CPTP map for the system S, one requires the factorized initial condition $\rho_{tot}(0) = \rho_S(0) \otimes \rho_B^{eq}$. Here $\rho_S(0) \in \mathcal{S}(\mathcal{H}_S)$ is some initial state of the system and $\rho_B^{eq} \in \mathcal{S}(\mathcal{H}_B)$ is the initial state of the bath. Concerning thermodynamics, we usually assume that the bath is in an equilibrium state at some inverse temperature β given by

$$\rho_B^{eq} = \frac{e^{-\beta \mathrm{H}_B}}{\mathrm{tr}[e^{-\beta \mathrm{H}_B}]}. \tag{2.37}$$

The reduced dynamics of the system can be given under certain conditions by a general master equation of the form

$$\frac{d}{dt}\rho_S(t) = -i[\mathrm{H}'_S(t), \rho_S(t)] + \mathcal{D}_t[\rho_S(t)], \tag{2.38}$$

where the first term on the r.h.s. gives the unitary evolution of the system S with the effective Hamiltonian $\mathrm{H}'_S(t) = \mathrm{H}_S(t) + \Delta(t)$, where $\Delta(t)$ is the Lamb shift in the energy of the system because of the coupling to the bath. The second term on the r.h.s. is the dissipator which is responsible for the non-unitary evolution of the system due to the interaction with the bath.

2.4.2 Average work, average heat and the first law

Once the density matrix of the system is obtained for a given time $t \geq 0$, we can calculate the expectation value of the internal energy stored in the system. For a given Hamiltonian $\mathrm{H}_S(t)$, the internal energy is obtained by

$$U(t) = \mathrm{tr}[\mathrm{H}_S(t)\rho_S(t)]. \tag{2.39}$$

Since the system is subjected to a time-dependent Hamiltonian as well as interaction with a heat bath, it can exchange energy in the form of work and heat. This means that the average internal energy is changing by time. Taking the derivative of the both sides of Eq. (2.39) with respect to time

yields

$$\frac{d}{dt}U(t) = \mathrm{tr}[(\frac{d}{dt}\mathrm{H}_S(t))\rho_S(t)] + \mathrm{tr}[\mathrm{H}_S(t)(\frac{d}{dt}\rho_S(t))]. \tag{2.40}$$

The first term on the r.h.s. of Eq. (2.40) gives the average power denoted by $P(t)$, while the second term is the average rate of heat dissipation denoted by $J(t)$. Furthermore, by using Eq. (2.37) one obtains a more detailed expression for $J(t)$ as

$$J(t) = \mathrm{tr}[\mathrm{H}_S(t)\mathcal{D}_t[\rho(t)]], \tag{2.41}$$

where we have used the fact that the trace of a commutator is zero.

The change in the average internal energy of the system over a time interval $[t_1, t_2]$ is defined by $\Delta U := U(t_2) - U(t_1)$. Integrating both sides of Eq. (2.40) gives

$$\Delta U = \int_{t_1}^{t_2} d\tau P(\tau) + \int_{t_1}^{t_2} d\tau J(\tau) = W + Q, \tag{2.42}$$

with W and Q being the average work and average heat, respectively. Eq.(2.42) in fact expresses the first law of thermodynamics derived for an open quantum system [47, 81, 82].

2.4.3 Entropy and the second law

The entropy corresponding to a given observable and a given state is related to the ability of gathering information by performing a measurement using the observable on the state. Consider an operator A with the spectral decomposition $\mathrm{A} = \sum_i a_i \left|a_i\right\rangle \left\langle a_i\right|$. Therefore, the probability of a given outcome a_i is $p_{a_i} = \mathrm{tr}[\rho \left|a_i\right\rangle \left\langle a_i\right|]$ and the entropy of the probability distribution concerning all the possible outcomes is given by

$$S_{\{A,\rho\}} = -\sum_i p_{a_i} \ln p_{a_i}, \tag{2.43}$$

where S is the Shannon entropy. Von Neumann has shown that for a given density matrix ρ the operator that commutes with ρ minimizes the entropy in Eq. (2.43). Thereby, entropy of a state ρ is determined by the von

Neumann entropy [83]

$$S_{vN}(\rho) := -\mathrm{tr}[\rho \ln \rho] = -\sum_i p_i \ln p_i, \tag{2.44}$$

where p_i are the eigenvalues of the density matrix ρ.

The von Neumann entropy is invariant upon unitary transformations, thus entropy of the total state is constant in time, i.e. $S_{vN}(\rho_{tot}(t)) = S_{vN}(\rho_{tot}(0))$. As we consider initial factorized condition $\rho_{tot}(0) = \rho_S(0) \otimes \rho_B^{eq}$, one has the relation

$$-\mathrm{tr}[\rho_{tot}(0) \ln \rho_{tot}(0)] = -\mathrm{tr}[\rho_S(0) \ln \rho_S(0)] - \mathrm{tr}[\rho_B^{eq} \ln \rho_B^{eq}]. \tag{2.45}$$

However, a similar relation may not hold for $t > 0$ due to the generation of correlations between the system and the bath. We are interested in the entropy change of the system that can be addressed as follows. Entropy is a state function, therefore we have

$$\Delta S_{vN}(\rho_S) := S_{vN}(\rho_S(t)) - S_{vN}(\rho_S(0)), \tag{2.46}$$

where the reduced state of the system is obtained by tracing over the bath's degrees of freedom, i.e., $\rho_S(t) = \mathrm{tr}_B[\rho_{tot}(t)]$. Using Eq. (2.45) and Eq. (2.46), one finds

$$\Delta S_{vN}(\rho_S) = -\mathrm{tr}[\rho_{tot}(t) \ln \rho_S(t)] + \mathrm{tr}[\rho_{tot}(t) \ln \rho_{tot}(t)] - \mathrm{tr}[\rho_B^{eq} \ln \rho_B^{eq}], \tag{2.47}$$

which can be simplified further to get [84]

$$\Delta S_{vN}(\rho_S) = S(\rho_{tot}(t) \| \rho_S(t) \otimes \rho_B^{eq}) - \mathrm{tr}_B[(\rho_B(t) - \rho_B^{eq}) \ln \rho_B^{eq}], \tag{2.48}$$

where $\rho_B(t) = \mathrm{tr}_S[\rho_{tot}(t)]$ and $S(\rho_1 \| \rho_2) = S_{vN}(\rho_1) - \mathrm{tr}[\rho_1 \ln \rho_2]$ is the relative entropy, denoting the distance (distinguishability) of two density matrices. According to Eq. (2.48), entropy change of the reduced system has two parts, namely $\Delta S_{vN}(\rho_S) = \Sigma_{irr} + \Sigma_{rev}$. The second term on the r.h.s. of Eq. (2.48) is the reversible entropy flow due to the exchange of heat with the bath, which by considering the exact expression for the equilibrium state of the bath can be rewritten as $\Sigma_{rev} = \beta Q(t)$. $\Sigma_{irr} = S(\rho_{tot}(t) \| \rho_S(t) \otimes \rho_B^{eq})$ denotes the irreversible entropy production within the system due to generation of correlations between the system and the bath [84]. Note that, since relative entropy is a non-negative quantity,

entropy production is always positive or zero, as governed by the second law of thermodynamics.

It is worth noting that the entropy production has an alternative definition given by [29, 85]

$$\bar{\Sigma}_{irr} = S(\rho_S(0)\|\rho_S^{eq}) - S(\rho_S(t)\|\rho_S^{eq}), \tag{2.49}$$

where ρ_S^{eq} is the invariant state of the dynamics, i.e. $\mathcal{L}_t[\rho_S^{eq}] = 0$. Authors in [84] have shown that the relation between this definition and the previous one reads

$$\Sigma_{irr} = \bar{\Sigma}_{irr} - \beta(\mathrm{tr}[\mathrm{H}_I\rho_{tot}(t)] - \mathrm{tr}[\mathrm{H}_I\rho_{tot}(0)]) \geq 0. \tag{2.50}$$

Although the latter definition is more practical as it is dealing only with the local reduced state of the system, it might be puzzling in some cases. In particular, it may become negative – as it is shown for a class of non-Markovian dynamics in [46] – when the generator does not have a well-defined steady state. Nonetheless, the latter definition is always non-negative when dealing with Markovian semigroup class of dynamical maps, which have a steady state of the Gibbs form [29].

2.4.4 Quantum thermal machines

General formulation

Quantum heat engines that work between two heat baths at different temperatures absorb energy from the hot bath in the form of heat and transfer a portion of this energy into the extractable work. A fundamental quantity in heat engines is their efficiency in transferring heat to work. Consider the net extractable work done by the working substance, given by $\langle W_{net}\rangle$. Since we deal with a closed cycle, the change in the internal energy of the system over a full cycle is zero and due the first law one concludes $\langle W_{net}\rangle = -\langle Q_{net}\rangle$, where $\langle Q_{net}\rangle$ is the overall heat transferred in a full cycle. If we also consider the net average heat absorbed from the hot bath during a full cycle denoted by $\langle Q_h\rangle$, efficiency of the cycle reads

$$\eta = \frac{\langle W_{net}\rangle}{\langle Q_h\rangle}. \tag{2.51}$$

For a cycle working between two thermal baths at temperatures T_c and T_h, the Carnot efficiency $\eta_c = 1 - T_c/T_h$ gives an upper bound on the efficiency. This bound corresponds to a reversible cycle, in which the least amount of heat must be dissipated into the cold bath in order to close the cycle. It has been shown, however, that efficiency of a cycle working with a non-thermal bath, namely a squeezed bath, may exceed the Carnot bound [86].

A heat cycle can be described generally by a product series of CPTP dynamical maps [39], i.e., $\Lambda_{n\tau\to(n+1)\tau} = \prod_{i=1}^{4} \Phi_i$, where τ is the duration (period) of the cycle and $n \in \mathbb{Z}^{0+}$. Each dynamical map Φ_i describes a stroke of the cycle. As the cycle is closed, it has a steady state relation $\Lambda_{n\tau\to(n+1)\tau}[\rho(n\tau)] = \rho(n\tau)$, where $\rho_0 \equiv \rho(n\tau)$. Thus, at the end of each period everything resets to its initial configuration. Considering an explicit cyclic dynamical map one can obtain the state of the working substance (WS) at a given time $n\tau \leq t \leq (n+1)\tau$ and calculate the energy flow in the form of work and heat.

Generally speaking, each stroke of a cycle can be associated to three different situations: coherent drive on the WS without dissipation, coherent drive together with dissipation, and pure dissipation. The first scenario is described by a unitary evolution. Due to isolation of the system in this case, the only source of energy exchange is the work pumped into the WS by the external drive. The third case, on the other hand, is described by a non-unitary dynamical map, which leads to dissipation of heat into the bath. Considering a situation in between, the second case corresponds to both nonzero work and nonzero heat. Having in mind these possibilities, let us discuss some well-known thermodynamic strokes.

Adiabatic process – In an adiabatic process, the WS is subjected to a very slow coherent drive while it is isolated from the heat bath. Hence the evolution of the WS is unitary and there is no change in the entropy of the system. In an ideal adiabatic process energy level populations $p_i(t) = \langle E_i(t)| \rho(t) |E_i\rangle$ remain invariant, where $|E_i(t)\rangle$ are the instantaneous energy levels. This means that if the state of the WS commutes with the Hamiltonian at the beginning of the process, i.e. $[\mathrm{H}(0), \rho(0)] = 0$, the same condition holds during the whole process, i.e. $[\mathrm{H}(t), \rho(t)] = 0$. Consider the spectral decomposition of the instantaneous Hamiltonian as $\mathrm{H}(t) = \sum_i E_i(t) |E_i(t)\rangle \langle E_i(t)|$. Thereby the rate of performing work on the WS during an adiabatic process is obtained by $P(t) = \sum_i p_i dE_i(t)/dt$. Since an ideal adiabatic process is ultimately slow, one has $dE_i(t)/dt \approx 0$ and the power vanishes.

Isochoric process – In an isochoric process the WS is brought into contact with a heat bath. The two interact until the WS finally reaches a thermal equilibrium with the bath. As the dynamics is non-unitary, the entropy of the WS changes during the isochoric process. However, work is zero due to lack of an external drive.

Isothermal process – An isothermal process corresponds to the case in which we drive the WS while it is coupled to a heat bath. As the name of the process suggests, during an ideal isothermal process the WS remains in the thermal equilibrium with bath. Thus, while the level populations vary in time, their ratio remains invariant. This ideal scenario requires again a very slow drive which keeps the WS close to equilibrium. Therefore, an ideal isothermal process has a vanishing output power.

Quantum Stirling cycle as a heat engine

The Stirling cycle includes two isothermal and two isochoric strokes. In classical Stirling heat engines, direct coupling to the heat baths during the isochoric strokes is usually replaced by interaction with an internal substance with high heat capacity named regenerator. The purpose of the regenerator is to absorb heat from the WS during the cooling isochoric stroke and transfer the exact amount of energy back to the WS during the heating isochor. This helps to minimize the waste heat and improve the efficiency. However, in this thesis we do not consider a regenerative setup, so the WS is directly coupled to the heat baths instead of the regenerator during the isochoric strokes. A Stirling cycle working as a heat engine is described as follows.

1- Isothermal stroke $a \to b$: The WS is subjected to external drive while it is coupled to the hot bath at an inverse temperature β_h. The Hamiltonian of the system is initially $\mathrm{H}(t_a) = \mathrm{H}_1$ and the state of the WS is the thermal state $\rho_a = e^{-\beta_h \mathrm{H}_1}/\mathrm{tr}[e^{-\beta_h \mathrm{H}_1}]$. The external drive changes the Hamiltonian slowly from H_1 to the final Hamiltonian $\mathrm{H}(t_b) = \mathrm{H}_2$, such that during the process the WS remains in an equilibrium state $\rho(t) = e^{-\beta_h \mathrm{H}(t)}/\mathrm{tr}[e^{-\beta_h \mathrm{H}(t)}]$, and finally reaches the state $\rho_b = e^{-\beta_h \mathrm{H}_2}/\mathrm{tr}[e^{-\beta_h \mathrm{H}_2}]$. The energy transferred during this process includes an average work $\langle W_{ab} \rangle$ done on the WS and an average heat $\langle Q_{ab} \rangle$ absorbed from the hot bath.

2- Isochoric stroke $b \to c$: The WS disconnects from the hot bath and

is brought into contact with the cold bath at an inverse temperature β_c. The two interact till the WS reaches thermal equilibrium with the cold bath, so the state of the WS at the end of the process is $\rho_c = e^{-\beta_c \mathrm{H}_2}/\mathrm{tr}[e^{-\beta_c \mathrm{H}_2}]$. As the Hamiltonian is fixed, the only energy transferred is an average heat $\langle Q_{bc} \rangle$ dissipated into the cold bath.

3- Isothermal stroke $c \to d$: The WS is subjected to external drive while it is coupled to the cold bath at the inverse temperature β_c. The Hamiltonian of the system is initially $\mathrm{H}(t_c) = \mathrm{H}_2$ and the state of the WS is the thermal state $\rho_c = e^{-\beta_c \mathrm{H}_2}/\mathrm{tr}[e^{-\beta_c \mathrm{H}_2}]$. The external drive changes the Hamiltonian slowly from H_2 back to $\mathrm{H}(t_d) = \mathrm{H}_1$, such that during the process the WS remains in the instantaneous equilibrium state. At the end of the process the WS is in the state $\rho_d = e^{-\beta_c \mathrm{H}_1}/\mathrm{tr}[e^{-\beta_c \mathrm{H}_1}]$. The energy transferred during this process includes an average work $\langle W_{cd} \rangle$ done by the WS and an average heat $\langle Q_{cd} \rangle$ dissipated to the cold bath.

4- Isochoric stroke $d \to a$: The WS disconnects from the cold bath and is brought back to interact with the hot bath at the inverse temperature β_h. At the end of the process, the WS reaches thermal equilibrium with the hot bath and the state of the WS comes back to its initial configuration at the beginning of the cycle, i.e. $\rho_a = e^{-\beta_h \mathrm{H}_1}/\mathrm{tr}[e^{-\beta_h \mathrm{H}_1}]$. As the Hamiltonian is fixed, the only energy transferred is an average heat $\langle Q_{da} \rangle$ absorbed from the hot bath.

According to the description above, the efficiency of the Stirling cycle is obtained by

$$\eta = \frac{-(\langle Q_{ab} \rangle + \langle Q_{bc} \rangle + \langle Q_{cd} \rangle + \langle Q_{da} \rangle)}{\langle Q_{ab} \rangle + \langle Q_{da} \rangle}. \tag{2.52}$$

The heat transferred during each stroke can be calculated analytically for an ideal Stirling cycle [87]. Recalling the relation between entropy change and the heat transferred at a constant temperature T given by $\Delta S = \int \langle \delta Q \rangle / T$, for an isothermal stroke $i \to j$ at the inverse temperature β one has

$$\langle Q_{i \to j} \rangle_{isothermal} = \beta^{-1}(S_{vN}(\rho_j) - S_{vN}(\rho_i)). \tag{2.53}$$

For an isochoric stroke at a fixed Hamiltonian H, the situation is easy as

the only way the system exchanges energy is in the form of heat, thus

$$\langle Q_{i\to j}\rangle_{isochoric} = \mathrm{tr}[\mathrm{H}\rho_j] - \mathrm{tr}[\mathrm{H}\rho_i]. \tag{2.54}$$

Chapter 3

Quantum information protocols with two-photon dephasing model

In this chapter, we concentrate on those results of the thesis that deal with implementation of quantum information protocols in presence of noise. Essential to the results is the two-photon dephasing model and implementation of non-local memory effects. Thus, we first give a brief overview of the model and then proceed to represent some original results concerning a master equation approach to the open dynamics. After this theoretical part, we discuss two protocols studied in the thesis. The first one gives a theoretical framework to remote generation of polarization entanglement by utilizing open system dynamics and interference. We note that an experimental realization of this protocol is currently in development. The peculiar mechanism allowing for generation of entanglement in this method is rooted in the quantum interference, for which we give a brief discussion preceding to the main results. The second protocol deals with the implementation of perfect teleportation with open quantum systems. This part contains some modification to the original theoretical proposal and, more importantly, the original experimental results realizing the modified protocol.

3.1 Photonic dephasing model

Photonic systems provide a controllable platform to implement and realize quantum information protocols. They are specifically interesting candidates to develop quantum communication networks [27]. Different degrees of

freedom of photons, e.g., polarization, spatial path, and orbital angular momentum, can be utilized to implement multi-qubit quantum systems [88], and they are also practical for simulating dynamics of open quantum systems [51, 89–91].

Among different dynamics that can be implemented by photonic systems, dephasing is the focus of the thesis. In the photonic dephasing model, polarization degrees of freedom of the photon is the open system and frequency degrees of freedom of the same photon act as the environment. Consider the initial polarization-frequency state

$$|\Psi(0)\rangle = |\psi(0)\rangle \otimes |\Omega\rangle \,, \tag{3.1}$$

where, $|\psi(0)\rangle$ is the initial polarization state on the Hilbert space $\mathcal{H}_p$ spanned by the horizontal-vertical polarization basis $\{|h\rangle \,, |v\rangle\}$, and

$$|\Omega\rangle = \int d\omega \; g(\omega) \, |\omega\rangle \,, \tag{3.2}$$

denotes the initial frequency state with $g(\omega)$ being the probability amplitude of the photon being at a given frequency ω. If the photon travels through a birefringent medium, like a quartz plate, its polarization and frequency interact due to the Hamiltonian ($\hbar = 1$)

$$\mathrm{H} = (n_h \, |h\rangle \langle h| + n_v \, |v\rangle \langle v|) \otimes \int d\omega \; \omega \, |\omega\rangle \langle \omega| \,, \tag{3.3}$$

where n_h (n_v) is the refraction index for polarization component h (v). Let the two degrees of freedom interact for a given time t. By tracing over the frequency degrees of freedom, the reduced dynamics of the polarization state will be obtained by a CPTP dynamical map $\rho(t) = \Phi_t[\rho(0)]$, such that

$$\rho(t) = \begin{pmatrix} \langle h| \, \rho(0) \, |h\rangle & \kappa(t) \, \langle h| \, \rho(0) \, |v\rangle \\ \kappa(t)^* \, \langle v| \, \rho(0) \, |h\rangle & \langle v| \, \rho(0) \, |v\rangle \, . \end{pmatrix} , \tag{3.4}$$

where $\rho(0) = |\psi(0)\rangle \langle \psi(0)|$. The dephasing dynamics is fully described by the decoherence function

$$\kappa(t) = \int d\omega \; |g(\omega)|^2 \mathrm{e}^{-i\Delta n \omega t}, \tag{3.5}$$

where $\Delta n = n_v - n_h$. We note that $0 \leq |\kappa(t)| \leq 1$ for all times $t \geq 0$ and $|\kappa(0)| = 1$. Besides the dynamical map approach, the dephasing model discussed above can be described by a master equation given by

$$\frac{d}{dt}\rho(t) = -i\frac{\nu(t)}{2}[\sigma_z, \rho(t)] + \frac{\gamma(t)}{2}[\sigma_z \rho(t) \sigma_z - \rho(t)], \tag{3.6}$$

where, σ_z is the Pauli z operator and the rates $\nu(t)$ and $\gamma(t)$ are obtained by

$$\gamma(t) = -\mathrm{Re}\left[\frac{1}{\kappa(t)}\frac{d\kappa(t)}{dt}\right], \quad \nu(t) = -\mathrm{Im}\left[\frac{1}{\kappa(t)}\frac{d\kappa(t)}{dt}\right], \tag{3.7}$$

with Re[·] and Im[·] indicating the real and imaginary parts, respectively.

3.1.1 Two-photon dephasing model: dynamical map

Experimentally, a pair of photons can be created in the nonlinear spontaneous parametric down conversion (SPDC) process. In this process the so-called *pump* photon with frequency ω_0 annihilates due to interaction with a nonlinear medium and results in the creation of two photons with frequencies ω_1 and ω_2. Due to conservation of energy, the frequencies of the created photons fulfill the relation $\omega_0 = \omega_1 + \omega_2$. However, since the pump source always has some finite frequency width, there is always some nonzero uncertainty in the sum of the frequencies of the created photons. Two different designs of this process, namely type-I and type-II SPDC, are widely being used to create entangled pairs of photons in the polarization degrees of freedom.

Besides providing a source of entangled particles, two-photon model has been used to implement nontrivial open system dynamics of bipartite quantum systems, specifically with dephasing [49, 50, 92]. To generalize the single-photon dephasing model discussed earlier to the two-photon case, consider a pair of photons labeled by a and b whose total polarization-frequency initial state reads

$$|\Psi_0\rangle = |\psi(0)\rangle \otimes \int d\omega_a \int d\omega_b \, g(\omega_a, \omega_b) \, |\omega_a, \omega_b\rangle \,, \tag{3.8}$$

where the initial two-photon frequency degrees of freedom has a joint-probability distribution $P(\omega_a, \omega_b) = |g(\omega_a, \omega_b)|^2$ and the two-photon polar-

ization Hilbert space is spanned by the bipartite basis $\{|\alpha\beta\rangle\}$, with $\alpha, \beta = h, v$. Letting polarization of each photon interact with its local frequency degrees of freedom for some time $t_{a(b)}$ with the Hamiltonian in Eq. (3.3), one obtains a unitary dynamics $\mathrm{U}(t_a, t_b) := \exp(t_a \mathrm{H}_a \otimes I_b + t_b I_a \otimes \mathrm{H}_b)$ which maps the total polarization-frequency state as $|\Psi(t_a, t_b)\rangle = \mathrm{U}(t_a, t_b)\,|\Psi_0\rangle$. Following the unitary dynamics of the total state, a reduced dynamical map for the two-photon polarization state will be obtained by tracing out the frequency degrees of freedom, i.e. $\rho(t_a, t_b) = \Phi_{ab}(t_a, t_b)[|\Psi_0\rangle\langle\Psi_0|] := \mathrm{tr}_\omega[|\Psi(t_a, t_b)\rangle\langle\Psi(t_a, t_b)|]$. Consequently, one gets [49, 50]

$$\rho(t_a, t_b) = \tag{3.9}$$
$$\begin{pmatrix} p_{hh,hh} & \kappa_b(t_b)p_{hh,hv} & \kappa_a(t_a)p_{hh,vh} & \kappa_{ab}(t_a,t_b)p_{hh,vv} \\ \kappa_b^*(t_b)p_{hv,hh} & p_{hv,hv} & \Lambda_{ab}(t_a,t_b)p_{hv,vh} & \kappa_a(t_a)p_{hv,vv} \\ \kappa_a^*(t_a)p_{vh,hh} & \Lambda_{ab}^*(t_a,t_b)p_{vh,hv} & p_{vh,vh} & \kappa_b(t_b)p_{vh,vv} \\ \kappa_{ab}^*(t_a,t_b)p_{vv,hh} & \kappa_a^*(t_a)p_{vv,hv} & \kappa_b(t_b)^*p_{vv,vh} & p_{vv,vv} \end{pmatrix}.$$

Here, we have defined $p_{\alpha\beta,\alpha'\beta'} = \langle\alpha\beta\,|\Psi(0)\rangle\langle\Psi(0)|\,\alpha'\beta'\rangle$ with $\alpha, \beta, \alpha', \beta' = h, v$. By recalling $\Delta n = n_v - n_h$, the local decoherence functions for the photon $j = a, b$ are given by

$$\kappa_j(t) = \int d\omega_a \int d\omega_b\; P(\omega_a, \omega_b)\mathrm{e}^{-i\Delta n\omega_j t}, \tag{3.10}$$

and the non-local ones – that appear in the two-photon dynamics, but not in the reduced dynamics of each photon – are expressed by

$$\kappa_{ab}(t_a, t_b) = \int d\omega_a \int d\omega_b\; P(\omega_a, \omega_b)\mathrm{e}^{-i\Delta n(\omega_a t_a + \omega_b t_b)}, \tag{3.11}$$

and

$$\Lambda_{ab}(t_a, t_b) = \int d\omega_a \int d\omega_b\; P(\omega_a, \omega_b)\mathrm{e}^{-i\Delta n(\omega_a t_a - \omega_b t_b)}. \tag{3.12}$$

Let us briefly elaborate some properties of the dynamics above. The reduced dynamics of each photon, obtained by $\rho_{a(b)}(t_{a(b)}) = \mathrm{tr}_{b(a)}[\rho(t_a, t_b)]$ is only dependent on the local decoherence functions $\kappa(t_i)$. Therefore, local dynamics of the photons are controlled by the marginal probability distributions $P_a(\omega_a) = \int d\omega_b P(\omega_a, \omega_b)$ and $P_b(\omega_b) = \int d\omega_a P(\omega_a, \omega_b)$. On the other hand, dynamics of the two-photon system is dependent on the

non-local decoherence functions κ_{ab} and Λ_{ab} in addition to the local decoherence functions κ_i. This means that if the joint frequency probability distribution does not factorize due to frequency-frequency correlations, i.e., $P(\omega_a, \omega_b) \neq P_a(\omega_a) \times P_b(\omega_b)$, the two-photon dynamical map given by Eq. (3.9) can not be written in a factorized form, i.e., $\Phi_{ab} \neq \Phi_a \otimes \Phi_b$ [49, 50].

It is therefore clear that the dynamics is highly dependent on the properties of the joint frequency probability distribution $P(\omega_a, \omega_b)$. For most experimental situations it is justifiable to model the joint frequency probability distribution with a bivariant Gaussian distribution. It is specifically handy to use Gaussian distributions since they are fully described by their first two moments, namely the mean and the variance. For a distribution $P(\omega_a, \omega_b)$ one defines covariance matrix $C = (C_{ij})$, such that $C_{ij} = \langle \omega_i \omega_j \rangle - \langle \omega_i \rangle \langle \omega_j \rangle$ for $i, j = a, b$. Frequency-frequency correlation is quantified by the so-called correlation coefficient $K = C_{ab}/\sqrt{C_{aa} C_{bb}}$, such that $-1 \leq K \leq 1$. Thus, a fully anti-correlated initial frequency distribution has $K = -1$, which results in $\omega_a + \omega_b \equiv \omega_0$, with some constant frequency ω_0. The mean frequency of the photons are given by the vector $(\bar{\omega}_a, \bar{\omega}_b)^{\mathrm{T}}$ and we introduce the separation between the local peaks by $\bar{\omega}_a - \bar{\omega}_b = \Delta\omega$ and their sum as $\bar{\omega}_a + \bar{\omega}_b = \omega_0$. This formulation let us gain some more intuition about the properties of the dynamics. We note that while the local decoherence functions κ_i do not depend on the correlation coefficient, the non-local decoherence functions are dependent on it. Especially, κ_{ab} shows an interesting property, such that when $K = -1$ one has $\omega_a + \omega_b \equiv \omega_0$ and $|\kappa_{ab}(t, t)| = 1$. This means that if the interaction times on two sides are identical and the frequency distribution is fully anti-correlated, the subspace spanned by $|hh\rangle$ and $|vv\rangle$ is a decoherence-free subspace. Now suppose a single-peak bivariate Gaussian frequency distribution. We first let the photon a dephase for some time $t_a = t$ while nothing happens for the other photon. In this case one finds that $|\kappa_{ab}(t, 0)| < 1$, so the coherence within the subspace spanned by $|hh\rangle$ and $|vv\rangle$ decreases. At this point, if we turn on the interaction for photon b for some interaction time $t_b \leq t$, we find that $|\kappa_{ab}|$ starts to increase. This means that the lost coherence revives, and consequently the dynamics has to be non-Markovian [49, 50]. Although the two-qubit polarization dynamics is non-Markovian, the reduced dynamics of each photon is still Markovian as the local dynamics are only dependent on the local decoherence functions.

3.1.2 Two-photon dephasing model: master equation

In addition to a CP map description of the dephasing dynamics given by Eq. (3.9), one can seek for a master equation description which sheds some more light on the relation between the properties of the frequency distribution and the polarization reduced dynamics. For the sake of simplicity, we set $t_a = t_b = t$ and define the corresponding CP map by Φ_t. Consider the generator of the map denoted by $\mathcal{L}_t$, which formally fulfills $\Phi_t = \exp\Big[\int_0^t d\tau \mathcal{L}_\tau\Big]$. The master equation we want to construct is given by

$$\frac{d}{dt}\rho(t) = \mathcal{L}_t[\rho(t)], \tag{3.13}$$

so the aim is to find an expression for $\mathcal{L}_t$ corresponding to the dynamics in Eq. (3.9). If Φ_t is invertible and its derivative is well-defined, we obtain the generator by

$$\mathcal{L}_t = \frac{d}{dt}\Phi_t \circ \Phi_t^{-1}. \tag{3.14}$$

A systematic way to calculate the generator is to provide a suitable matrix representation for Eq. (3.14) with regards to a complete operator basis on $\mathcal{S}(\mathcal{H}_4)$, where $\mathcal{H}_4$ is the 4-dimensional Hilbert space of the two-photon polarization. Let us choose the set of operator basis constituted by the fifteen generators of SU(4) plus $\mathrm{F}_1 = \mathrm{I}/\sqrt{4}$, such that $\mathrm{Tr}[\mathrm{F}_i^\dagger \mathrm{F}_j] = \delta_{ij}$. Therefore, the operatorial relation in Eq. (3.14) will be transformed to a matrix relation

$$[\mathcal{L}_t] = \frac{d}{dt}[\Phi_t].[\Phi_t]^{-1}. \tag{3.15}$$

To obtain an explicit expression for the generator, we consider a general Lindblad form. Recalling the operator basis $\{\mathrm{F}_i\}$, we have

$$\mathcal{L}_t[\rho(t)] \;\; = -i[\mathrm{H}(t), \rho(t)] + \sum_{\alpha=2}^{16}\sum_{\beta=2}^{16} R_{\alpha\beta}(t)\Big(\mathrm{F}_\alpha \rho(t) \mathrm{F}_\beta^\dagger - \frac{1}{2}\{\mathrm{F}_\beta^\dagger \mathrm{F}_\alpha, \rho(t)\}\Big), \tag{3.16}$$

where

$$\mathrm{H}(t) = \frac{-1}{2i}\sum_{\alpha=2}^{16}\Big[R_{\alpha 1}(t)\mathrm{F}_\alpha - R_{1\alpha}(t)^*\mathrm{F}_\alpha^\dagger\Big], \tag{3.17}$$

and R is a 15×15 matrix whose elements $R_{\alpha\beta}\in\mathbb{R}$ give the transition rates of the master equation. Consequently, a matrix representation of the generator will be obtained by

$$[\mathcal{L}_t]_{\alpha\beta} = \mathrm{Tr}[\mathrm{F}_\alpha^\dagger\mathcal{L}_t[\mathrm{F}_\beta]]. \tag{3.18}$$

By elementwise comparison of Eq. (3.18) and Eq. (3.15) one finds the rates of the master equation in Eq. (3.16) in terms of the decoherence functions in Eqs. (3.10-3.12). It turns out that the rate matrix has only a 3×3 non-zero subspace. If we diagonalize this matrix, the second term on the r.h.s of Eq. (3.16) – which encapsulates the non-unitary dynamics – simplifies to

$$\mathcal{D}[\rho(t)] = \sum_{\alpha=1}^{3}\gamma_\alpha(t)\Big[\mathrm{J}_\alpha\rho(t)\mathrm{J}_\alpha^\dagger - \frac{1}{2}\{\mathrm{J}_\alpha^\dagger\mathrm{J}_\alpha,\rho(t)\}\Big]. \tag{3.19}$$

Naturally, the rates γ_i and the operators J_i are dependent on the joint frequency distribution $P(\omega_a,\omega_b)$. One specific distribution that is experimentally realizable and is utilized in this thesis is constituted by sum of two single-peak Gaussian distributions, i.e., $P(\omega_a,\omega_b)=\sum_{i=1}^{2}P_i(\omega_a,\omega_b)/2$. Let the two have the mean value vectors $(\omega_0/2-\Delta\omega/2,\omega_0/2+\Delta\omega/2)^{\mathrm{T}}$ and $(\omega_0/2+\Delta\omega/2,\omega_0/2-\Delta\omega/2)^{\mathrm{T}}$, identical standard deviation vectors $(\sigma,\sigma)^T$, and identical correlation coefficient K. Accordingly, the decay rates and operators in Eq. (3.19) will be obtained respectively as

$$\gamma_1(t) = 2(1-K)\sigma^2\Delta n^2 t + \tan(t\Delta n\Delta\omega)\Delta n\Delta\omega, \tag{3.20}$$

$$\gamma_2(t) = 2(1+K)\sigma^2\Delta n^2 t, \tag{3.21}$$

$$\gamma_3(t) = \frac{1}{2}\tan\left(\frac{t\Delta n\Delta\omega}{2}\right)\big[1-\sec(t\Delta n\Delta\omega)\big]\Delta n\Delta\omega, \tag{3.22}$$

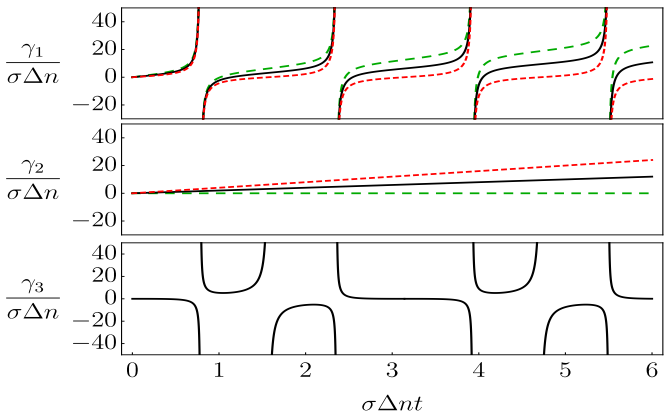

Figure 3.1: Transition rates of the master equation plotted as a function of the interaction time. Dashed green lines indicate $K = -1$, solid black lines for $K = 0$, and dot-dashed red lines when $K = 1$. Here we set $\Delta\omega/\sigma = 2$.

and

$$\mathrm{J}_1 = \frac{1}{2\sqrt{2}}(\mathrm{I}_2 \otimes \sigma_z + \sigma_z \otimes \mathrm{I}_2), \tag{3.23}$$

$$\mathrm{J}_2 = \frac{1}{2\sqrt{2}}(\mathrm{I}_2 \otimes \sigma_z - \sigma_z \otimes \mathrm{I}_2), \tag{3.24}$$

$$\mathrm{J}_3 = \frac{1}{2}\sigma_z \otimes \sigma_z. \tag{3.25}$$

The explicit expressions of the decay rates are clearly dependent on the properties of P. If the two single-peak Gaussian distributions are identical, i.e., $\Delta\omega = 0$, we always have $\gamma_3 = 0$. This means that with a single-peak Gaussian distribution the channel governed by the operator J_3 is absent and dynamics is solely governed by the local operators J_1 and J_2. Interestingly, with a single-peak distribution the decay rates are always non-negative, and the dynamics is Markovian. In contrary, whenever $\Delta\omega \neq 0$ the first and third rates can take negative values, indicating a non-Markovian dynamics. Furthermore, one realizes that while γ_3 is independent of K and σ, the other two rates are functions of the local correlation coefficient and width of the distribution. Specifically, with a fully anti-correlated distribution ($K = -1$), the second rate always vanishes, whereas, γ_1 vanishes with

$K = 1$ and $\Delta\omega = 0$. A special situation happens with $\Delta\omega = 0$ and uncorrelated frequency distribution with $K = 0$, when one has $\gamma_1 = \gamma_2$ and $\gamma_3 = 0$. One can check that in this case the generator is fully local and the dynamical map factorizes, i.e. $\Phi_{ab} = \Phi_a \otimes \Phi_b$. The other striking feature is that γ_1 and γ_3 diverge at some isolated points in time, as depicted in Fig. (3.1). This may suggest that the map is not invertible and therefore the master equation obtained is not valid. Nonetheless, we note that the divergence happens at some isolated points at which the elements of the generalized Bloch vector of the two-photon polarization state, given by $r_i(t) = \mathrm{tr}[\mathrm{F}_i\rho(t)]$, happen to be zero. Therefore, the product of divergent rates and zero inputs provides a finite rate of change of the Bloch vector, which allows us to follow the evolution of the state unambiguously.

3.2 Interference-induced generation of entanglement

In chapter 2, we introduced a general interferometric approach that involves any quantum system with a finite and discrete Hilbert space. An interesting situation considering this general picture arises when the system or the detector coupled to it are multipartite. Suppose we use a generalized beam splitter (or any other method) to overlap the paths of an interferometer. What happens then if the detector is a two-qubit system? This actually can lead to generation of entanglement. The idea of superposing different states of a multipartite system to generate entanglement has been reported for example in [93, 94]. However, an interferometric formulation has not been explored so far. By adapting the simplest scenario, we roughly discuss the requirements for entanglement generation with interference and leave a generic formulation for later studies. We proceed then to present our results for polarization-entanglement generation using the two-photon dephasing model and interference in frequency domain.

3.2.1 The simplest case: 2-port interferometer and a two-qubit system as the detector

Presume a hypothetical two-port interferometer with the paths denoted by the orthogonal vectors $|0\rangle$ and $|1\rangle$ on the Hilbert space $\mathcal{H}_I$. We recall that these two vectors need not to be associated only with spatial degrees of

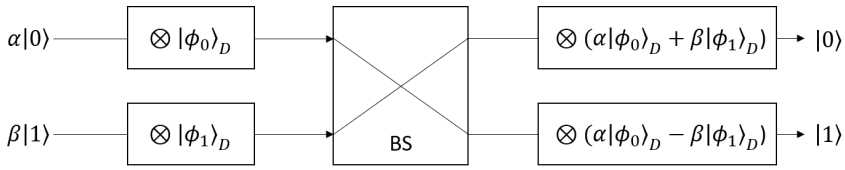

Figure 3.2: An interferometer with two ports 0 and 1. The beam splitter (BS) makes a 50/50 superposition of the two paths. As a consequence, the two detector states $|\phi_0\rangle_D$ and $|\phi_1\rangle_D$ that have been coupled respectively to $|0\rangle_I$ and $|1\rangle_I$ superpose.

freedom. Thus, in general there might be no actual particle or a physically existing interferometer, but rather it is just the state vector of a quantum system spanned by the two vector bases. Nonetheless, to help comprehending the situation we assume an actual interferometer depicted in Fig. 3.2, with the two paths $|0\rangle$ and $|1\rangle$. A hypothetical particle inside the interferometer takes a general pure state $|\psi\rangle = \alpha\,|0\rangle_I + \beta\,|1\rangle_I$, with $|\alpha|^2 + |\beta|^2 = 1$. Now consider a two-qubit system as a detector labeling the paths of the interferometer by building correlation with it. The 4-dimensional Hilbert space of the detector is denoted by $\mathcal{H}_D = \mathcal{H}_{D_1} \otimes \mathcal{H}_{D_2}$, which is spanned by the four orthogonal vectors $\{|00\rangle_D, |01\rangle_D, |10\rangle_D, |11\rangle_D\}$. From the elements of this set only two vectors would be enough to get full which-path information. Nonetheless, our goal here is not labeling the paths, but rather generation of entanglement in the detector system. Assume the detector is initially in a global state $|\phi_g\rangle$ and after the interaction with the interferometer the total state evolves to

$$|\Psi\rangle = \alpha\,|0\rangle_I \otimes |\phi_0\rangle_D + \beta\,|1\rangle_I \otimes |\phi_1\rangle_D\,. \tag{3.26}$$

The which-path information (system-detector correlation) is maximum when $\langle\phi_0|\phi_1\rangle = 0$. Let us now put a 50/50 beam splitter on the way of the two paths. For example consider applying a Hadamard gate H on the two vectors $|0\rangle$ and $|1\rangle$, such that $\mathrm{H}\,|0\rangle = \frac{1}{\sqrt{2}}(|0\rangle + |1\rangle)$ and $\mathrm{H}\,|1\rangle = \frac{1}{\sqrt{2}}(|0\rangle - |1\rangle)$. Due to overlapping of the two paths, the state vectors $|\phi_i\rangle_D$ superpose in

the output paths of the interferometer, such that

$$\mathrm{H}\,|\Psi\rangle = \frac{1}{\sqrt{2}}[\,|0\rangle_I \otimes (\alpha\,|\phi_0\rangle_D + \beta\,|\phi_1\rangle_D) + |1\rangle_I \otimes (\alpha\,|\phi_0\rangle_D - \beta\,|\phi_1\rangle_D)]. \tag{3.27}$$

Consequently, detecting the system at either of the output ports $0, 1$ gives a superposition of the two detector state vectors $|\phi_0\rangle_D$ and $|\phi_1\rangle_D$. The intuitive question thus is whether the resulting states $|\phi_\pm\rangle_D := \alpha\,|\phi_0\rangle_D \pm \beta\,|\phi_1\rangle_D$ contains entanglement.

Let $|\phi_i\rangle_D = a_i\,|00\rangle_D + b_i\,|01\rangle_D + c_i\,|10\rangle_D + d_i\,|11\rangle_D$. Accordingly, one has

$$|\phi_\pm\rangle_D = A_\pm\,|00\rangle_D + B_\pm\,|01\rangle_D + C_\pm\,|10\rangle_D + D_\pm\,|11\rangle_D\,, \tag{3.28}$$

where $X_\pm := \alpha \mathrm{x}_0 \pm \beta \mathrm{x}_1$. Entanglement of these states depends on all of the amplitudes involved in the total state in Eq. (3.26). These amplitudes also determine the distribution of correlations among the interferometer and the detector before the action of the beam splitter. In particular, consider

$$\begin{aligned}|\Psi\rangle = \frac{1}{2\sqrt{2}}[\,&|0\rangle_I \otimes (|00\rangle_D + |01\rangle_D + |10\rangle_D + |11\rangle_D) \\ &+ |1\rangle_I \otimes (|00\rangle_D - |01\rangle_D - |10\rangle_D + |11\rangle_D)].\end{aligned} \tag{3.29}$$

The state above includes maximal entanglement between the interferometeric paths and the two-qubit detector system. However, the reduced states $\rho_{ID_1} = \mathrm{tr}_{D_2}[|\Psi\rangle\langle\Psi|]$ and $\rho_{ID_2} = \mathrm{tr}_{D_1}[|\Psi\rangle\langle\Psi|]$ contain no entanglement, which is expected considering the monogamy of entanglement [95]. Now applying the Hadamard transformation results in

$$\mathrm{H}\,|\Psi\rangle = \frac{1}{2}[|0\rangle_I \otimes (|00\rangle_D + |11\rangle_D) + |1\rangle_I \otimes (|01\rangle_D + |10\rangle_D)]. \tag{3.30}$$

Thus measuring the system on either of the paths $0, 1$ provides a maximally entangled state of the two-qubit detector system.

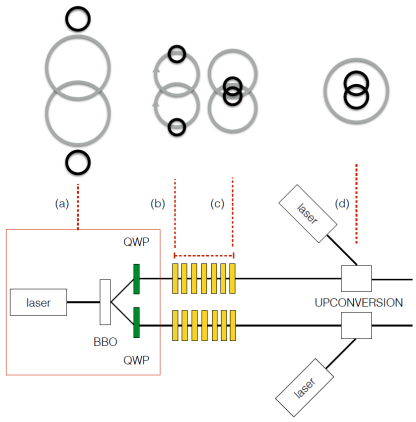

Figure 3.3: A schematic description of the protocol and the corresponding optical set-up. (a) The initial total state of the photon pair is prepared in a spontaneous parametric down-conversion process, such that the polarization state (black circles) is factorized, while the frequency state (grey circles) is entangled due to narrow frequency width of the laser pump. (b) When the photons travel through quartz plates, their polarization become coupled with the frequency. (c) The length of the quartz plates (so the interaction time) is fixed to prepare the desired total state. (d) The distinguishability of the frequency paths is erased due to frequency up-conversion and interference happens in frequency domain.

3.2.2 Remote polarization-entanglement generation by local dephasing and frequency up-conversion

We introduce an experimentally realizable protocol to implement interference-induced generation of entanglement based on the two-photon dephasing model, pictorially depicted in Fig. 3.3. In this scenario, frequency degrees of freedom of the photons provide the interferometric paths and polarization of the photon pair corresponds to the two-qubit detector system in which we want to create entanglement. The first crucial step is to control polarization-frequency correlation by manipulating the two-qubit polarization state coupled to each frequency path. This can be done by local dephasing dynamics of each photon. The second step is to overlap the frequency paths to enable the interference. We do so by erasing distin-

guishability of frequency paths by local frequency up-conversion of each photon. As the whole protocol is relying only on the local operations, it can be used to generate entanglement between distant photons.

Although the main mechanism of this protocol is similar to what we discussed using the 2-port interferometer, there are also some complications involved in comparison to that toy model. First of all, frequency degrees of freedom is continuous, hence we deal with infinite frequency paths. Second, instead of making a superposition of different paths in order to enable interference, we erase distinguishability of the paths by frequency up-conversion and make them overlap. Consider the initial total state of the photon pair given by

$$|\Psi_0\rangle = \frac{1}{2}\int d\omega_a \int d\omega_b g(\omega_a,\omega_b)\,|\omega_a,\omega_b\rangle \otimes \big(\,|hh\rangle + |hv\rangle + |vh\rangle + |vv\rangle\,\big). \tag{3.31}$$

Comparing this state with Eq. (3.26), we associate each vector $|\omega_a,\omega_b\rangle$ with a path of a hypothetical interferometer. At this stage, the polarization reduced state is separable and it contains no correlation with the frequency paths. To prepare the desired correlation between the frequency paths and the polarization of the photon pair we use local dephasing dynamics with identical interaction times $t_a = t_b = t$. We recall that, although the dephasing interactions are local for each photon, the overall dynamical map of the two-qubit polarization system will be non-local if the initial frequency distribution is correlated. After the local interactions, the total state of the photon pair evolves to

$$|\Psi_t\rangle = \frac{1}{2}\int d\omega_a d\omega_b g(\omega_a,\omega_b)\,|\omega_a,\omega_b\rangle \otimes \big(e^{itn_h(\omega_a+\omega_b)}\,|hh\rangle + e^{it(n_h\omega_a+n_v\omega_b)}\,|hv\rangle + e^{it(n_v\omega_a+n_h\omega_b)}\,|vh\rangle + e^{itn_v(\omega_a+\omega_b)}\,|vv\rangle\,\big). \tag{3.32}$$

The distribution of correlations between different parties in the state above depends on the properties of the frequency distribution $|g(\omega_a,\omega_b)|^2$ and also on the interaction time t. At this stage we take it as general as it is and proceed to discuss how to overlap different frequency paths. We use frequency up-conversion, where the pump photon with frequency ω_p and a local photon with frequency ω_i are annihilated to create a photon with higher frequency $\omega_o = \omega_i + \omega_p$. Generally speaking, the up-conversion pump

has a frequency distribution $P(\omega_p)$ with a finite width. Therefore, the output frequency follows the frequency distribution of the pump. Accordingly, frequency up-conversion results in the local map

$$|\omega_i\rangle \to \int d\omega_p P(\omega_p) \, |\omega_p + \omega_i\rangle \, , \tag{3.33}$$

which adds some uncertainty to the initial frequency. To make it clear assume two orthogonal vectors $|\omega_a, \omega_b\rangle$ and $|\omega'_a, \omega'_b\rangle$. The overlap of these vectors after local frequency up-conversion with identical pump distribution $P(\omega_p)$ is given by $E(\omega_a - \omega'_a) \times E(\omega_b - \omega'_b)$, where

$$E(\nu) = \int d\omega_p P(\omega_p) P(\omega_p + \nu). \tag{3.34}$$

For example if the pump photon has a normal distribution with width σ_p, we get $E(\nu) = \exp(-\nu^2/4\sigma_p^2)/(2\sigma_p\sqrt{\pi})$. The range of $\omega_i - \omega'_i$ is restricted by the width of the frequency distribution of the photon pair. Interestingly, for $\omega_i - \omega'_i \ll \sigma_p$ overlap of the up-converted frequency paths approaches to a non-zero constant, which means their distinguishability has been erased.

Suppose that all the frequency paths overlap idealistically. Thus, the frequency degrees of freedom in Eq. (3.32) would be factorized from the polarization reduced state. Nonetheless, the phases generated during the local dephasing dynamics still exist and combine to get

$$\begin{aligned} |\psi\rangle \propto \int d\omega_a d\omega_b g(\omega_a, \omega_b) (e^{itn_h(\omega_a+\omega_b)} \, |hh\rangle + e^{it(n_h\omega_a + n_v\omega_b)} \, |hv\rangle \\ + e^{it(n_v\omega_a + n_h\omega_b)} \, |vh\rangle + e^{itn_v(\omega_a+\omega_b)} \, |vv\rangle \,). \end{aligned} \tag{3.35}$$

Interestingly, if the initial frequency distribution of the photon pair is maximally anti-correlated ($\omega_a + \omega_b \equiv \omega_0$ for all given pair of frequencies) the integration over all the phases for the subspace spanned by $|hh\rangle$ and $|vv\rangle$ results in a constant relative phase. This also means that this subspace has not been correlated with the frequency degrees of freedom before the up-conversion. However, the result for the orthogonal subspace will be a decaying function of the width of the distribution and interaction time. In other words, while the interference for the former subspace is constructive, it is destructive for the latter subspace. This fact let us ultimately empty the amplitude of the $|hv\rangle + |vh\rangle$ subspace and get an entangled polarization state.

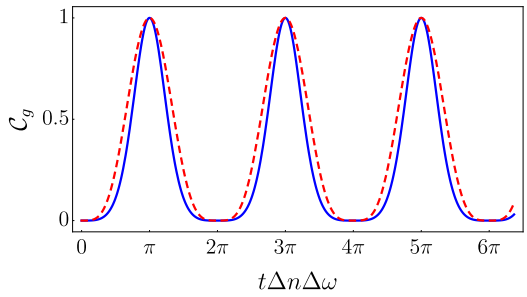

Figure 3.4: Concurrence of the reduced polarization state after mapping the frequency paths (generated entanglement) plotted in solid blue as a function of effective interaction time. Dashed-red line is $\Delta\mathcal{E}$.

The initial frequency-frequency correlation is crucial in the current protocol. If $k > -1$, the sum of the frequencies of the two photons is not constant and the subspace spanned by $|hh\rangle$ and $|vv\rangle$ does not remain factorized from the frequency paths. This means that destructive interference due to the sum of out of tuned phases happens also for this subspace and we do not have a desired control over the two-qubit polarization vectors. In fact, non-locality of the two-photon dephasing dynamics (due to initial frequency-frequency correlation) is a resource here. Although the non-local dephasing dynamics can not create polarization entanglement, it provides the rightful distribution of correlation within the total system that enables us to generate entanglement by interference.

To clarify this point we use a toy model in which the initial frequency distribution is fully correlated and is made of two sharp peaks $|\omega_1, \omega_2\rangle$ and $|\omega_2, \omega_1\rangle$ with $\omega_1 + \omega_2 = \omega_0$ and $\omega_1 - \omega_2 = \Delta\omega$. Thus, the total state can be considered a three-qubit system: one for the frequency degrees of freedom labeled by Q_f and two-qubit polarization state labeled by Q_{p_1} and Q_{p_2}. After local dephasing for some identical interaction times $t_a = t_b = t$, the total state reads

$$|\Psi_t\rangle = \frac{e^{in_h\omega_0 t}}{2\sqrt{2}}\Big[\,|\omega_1,\omega_2\rangle \otimes \big(\,|hh\rangle + e^{i\Delta n\omega_2 t}\,|hv\rangle + e^{i\Delta n\omega_1 t}\,|vh\rangle + e^{i\Delta n\omega_0 t}\,|vv\rangle\,\big) + |\omega_2,\omega_1\rangle \otimes \big(\,|hh\rangle + e^{i\Delta n\omega_1 t}\,|hv\rangle + e^{i\Delta n\omega_2 t}\,|vh\rangle + e^{i\Delta n\omega_0 t}\,|vv\rangle\big)\Big]. \tag{3.36}$$

Assume perfect mapping of the two frequency vectors to some fixed vector $|\omega_u, \omega_u\rangle$, which removes the frequency-polarization correlation and let the polarization vectors interfere. Before the frequency mapping, the distribution of entanglement in the three-qubit system fulfills the monogamy of entanglement, i.e., $\mathcal{C}(\rho_{fp_1})^2 + \mathcal{C}(\rho_{fp_2})^2 \leq \mathcal{C}(\rho_{f(p_1p_2)})^2$, with ρ_{xy} being the two-qubit reduced state obtained by tracing $|\Psi_t\rangle\langle\Psi_t|$ over the third qubit and $\mathcal{C}$ being the concurrence. As depicted in Fig. 3.4, an interesting observation is that the generated entanglement is upper-bounded by the residual entanglement of the three-qubit system before the frequency mapping, defined by $\Delta\mathcal{E} = \mathcal{C}(\rho_{f(p_1p_2)})^2 - \mathcal{C}(\rho_{fp_1})^2 - \mathcal{C}(\rho_{fp_2})^2$. For example, when $e^{i\Delta n\omega_1 t} = -e^{i\Delta n\omega_2 t}$ there is maximal correlation between Q_f and the two-qubit system $Q_{p1} \otimes Q_{p2}$, but the frequency paths are not entangled with the polarization of each photon separately. This means that $\mathcal{C}(\rho_{f(p_1p_2)})^2 = 1$ and $\mathcal{C}(\rho_{fp_1})^2 = \mathcal{C}(\rho_{fp_2})^2 = 0$. Exactly at this point we get the highest value of entanglement generation since the amplitude of $|hv\rangle + |vh\rangle$ is zero due to the completely destructive interference.

3.3 Perfect teleportation with open quantum systems

In reality, implementing the quantum teleportation protocol has to deal with a main challenge. As the time scale of the protocol is usually larger than the decoherence time of the qubits, the noisy channels have enough time to deteriorate the initial entanglement shared between Alice and Bob. By decreasing the entanglement, the fidelity of the teleported state decreases too. It has been shown that the maximum fidelity that can be achieved by using a fully mixed state and local operations and classical communication (LOCC) is 2/3 [96]. Nonetheless, it is shown that harnessing non-local memory effects allows for a high-fidelity teleportation protocol even with mixed states [53]. In what follows we present a modified version of the original protocol introduced in [53], and present a corresponding experimental realization.

3.3.1 Theoretical description

The protocol contains the following steps. Assume Alice and Bob initially share the maximally correlated polarization state $|\phi^+\rangle_{ab} = \frac{1}{\sqrt{2}}(|hh\rangle + |vv\rangle)$.

The total state of the photon pair with respect to the polarization and frequency degrees of freedom is given by

$$|\psi(0)\rangle = |\phi^+\rangle_{ab} \otimes \int d\omega_a \int d\omega_b g(\omega_a, \omega_b) \, |\omega_a, \omega_b\rangle \, . \tag{3.37}$$

The protocol begins with local dephasing dynamics on Alice's side. After Alice's photon went through a dephasing evolution for some time t_a, the total polarization state shared between Alice and Bob gets mixed, so we lose the entanglement resource in the polarization degrees of freedom.

After the local noise, Alice prepares the state she wants to send to Bob as $|\phi\rangle_s = \alpha \, |0\rangle + \beta \, |1\rangle$ on the spatial degrees of freedom of her photon. One can rewrite the full quantum state with respect to the path-polarization Bell states of photon a, such that

$$\begin{aligned} |\Psi(t_a)\rangle &= \frac{1}{2} \, |\Phi^+\rangle_{sa} \, [\alpha \, |h\rangle_b \, |\xi_{hh}(t_a)\rangle + \beta \, |v\rangle_b \, |\xi_{vv}(t_a)\rangle] \\ &+ \frac{1}{2} \, |\Phi^-\rangle_{sa} \, [\alpha \, |h\rangle_b \, |\xi_{hh}(t_a)\rangle - \beta \, |v\rangle_b \, |\xi_{vv}(t_a)\rangle] \\ &+ \frac{1}{2} \, |\Psi^+\rangle_{sa} \, [\beta \, |h\rangle_b \, |\xi_{hh}(t_a)\rangle + \alpha \, |v\rangle_b \, |\xi_{vv}(t_a)\rangle] \\ &+ \frac{1}{2} \, |\Psi^-\rangle_{sa} \, [\alpha \, |v\rangle_b \, |\xi_{vv}(t_a)\rangle - \beta \, |h\rangle_b \, |\xi_{hh}(t_a)\rangle], \end{aligned} \tag{3.38}$$

where $|\Phi^\pm\rangle_{sa} = \frac{1}{\sqrt{2}}(|0\rangle \, |H\rangle \pm |1\rangle \, |V\rangle)$ and $|\Psi^\pm\rangle_{sa} = \frac{1}{\sqrt{2}}(|0\rangle \, |V\rangle \pm |1\rangle \, |H\rangle)$ and $|\xi_{\lambda\lambda}(t_a)\rangle = \int d\omega_a d\omega_b g(\omega_a, \omega_b) e^{in_\lambda^a \omega_a t_a} \, |\omega_a, \omega_b\rangle$, with $\lambda = h, \; v$. Now Alice performs the polarization-path Bell-state measurement (BSM) on her photon and communicates the outcome result to Bob, whose local state collapses into one of the four possibilities. A standard teleportation protocol would be completed then if Bob applies a unitary operation to his photon (corresponding to the measurement outcome). However, the achieved fidelity will be limited due to the local noise on the Alice's side.

The situation can be different if we employ non-local memory effects induced by correlation between the frequencies of the two photons. After doing the Bell-state measurement, Alice's photon is eliminated and its frequency degrees of freedom do not exist anymore. This means that the information available in the local frequency state is discarded and we need to take the trace over ω_a. Assume that Alice's outcome has been $|\Phi^+\rangle_{sa}$,

thus, Bob's reduced polarization state collapses to

$$\rho_b = |\alpha|^2 |h\rangle\langle h| \otimes \rho_{hh} + \alpha\beta^* |h\rangle\langle v| \otimes \rho_{hv} + \alpha^*\beta |v\rangle\langle h| \otimes \rho_{vh} + |\beta|^2 |v\rangle\langle v| \otimes \rho_{vv}, \quad (3.39)$$

with

$$\begin{aligned} \rho_{hh} &= \int d\omega_b d\omega_b' d\omega_a g(\omega_a, \omega_b) g^*(\omega_1, \omega_b') |\omega_b\rangle\langle\omega_b'| = \rho_{vv}, \\ \rho_{hv} &= \int d\omega_b d\omega_b' \tilde{g}(\omega_b, \omega_b') |\omega_b\rangle\langle\omega_b'| = \rho_{vh}^\dagger, \end{aligned} \quad (3.40)$$

and $\tilde{g}(\omega_b, \omega_b') = \int d\omega_a g(\omega_a, \omega_b) g^*(\omega_a, \omega_b') e^{-i\Delta n_a \omega_a t_a}$. The state above is already correlated between polarization and frequency of Bob's photon, despite the fact that no local noise has been applied on Bob's side yet. The peculiar thing happens if Bob also subjects his photon to a local dephasing dynamics for a duration t_b. Interestingly, when the initial joint frequency distribution is correlated, the Bell-state measurement followed by the classical communication allows Bob's local polarization state to be affected not by the local decoherence function κ_b, but by the non-local decoherence function κ_{ab} defined in Eq. (3.11), such that

$$\begin{aligned} \rho_{\mathrm{b}} &= |\alpha|^2 |h\rangle\langle h| + \alpha\beta^* \kappa_{ab}(t_a, t_b) |h\rangle\langle v| \\ &\quad + \alpha^*\beta \kappa_{ab}(t_a, t_b)^* |v\rangle\langle h| + |\beta|^2 |v\rangle\langle v|. \end{aligned} \quad (3.41)$$

We already presented a formulation of the frequency distribution by the bivariant Gaussian distribution. Suppose a bivariant Gaussian distribution with correlation coefficient K, symmetric standard deviation vector $(\sigma, \sigma)^T$ and mean vector $(\omega_0/2, \omega_0/2)$. We know that whenever $K = -1$, one has $|\kappa_{ab}(t,t)| = 1$. Therefore, the only thing Bob needs to do is to set the dephasing time on his side to $t_b = t_a = \tau$ to get the pure state $|h\rangle + e^{i\tau\Delta n\omega_0} |v\rangle$. The extra phase factor would be eliminated easily by a local unitary on Bob's side and the teleportation is done perfectly. Note that, for all of the four possible outcomes of the BSM, Bob can complete the protocol perfectly. He just needs to apply the corresponding unitary gates (as done in a standard protocol) and then add the dephasing noise with the same duration, but with the difference that if the outcome is $|\Psi^\pm\rangle$ he must consider $\Delta n_b = -\Delta n_a$.

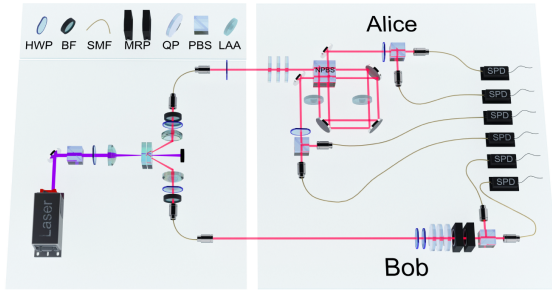

Figure 3.5: Realized experimental setup of the high-fidelity teleportation protocol with non-Markovian open system. The legend for the optical components used in the setup: HWP: half wave plate, BF: bandpass filter, SMF: single mode fiber, MRP: motor rotating plate, QP: Quartz plate, PBS: polarizing beam splitter, LAA: linear adjustable attenuator, SPD: single photon detector.

3.3.2 Experimental realization

The realized photonic setup for implementing the teleportation protocol with open quantum systems is illustrated in Fig. 3.5. A pair of polarization entangled photons are created in the type-I spontaneous parametric down-conversion process. The photon pair is also correlated in frequency due to the narrow width of the down-conversion laser pump. Using 3nm full width at half maximum bandpass filters, we prepare finite local frequency width for the photons with the peaks at 808nm. Then to implement the dephasing noise (on Alice's side or on the other side) we put quartz plates with specific thicknesses that correspond to the desired interaction times. The state to be teleported is prepared by employing the path degrees of freedom of Alice's photon in a specific Sagnac interference ring, which also allows for path-polarization Bell-state measurement. The ring contains a specific component called NPBS that is half beam splitter (BS) and half polarization beam splitter (PBS). To prepare the desired state of Alice we use linear adjustable attenuator (LAA) that allows for adjusting arbitrary amplitude ratio of the two paths of Alice. The polarization-path Bell-state measurement is done by overlapping the two paths of Alice in the PBS half of the specific beam splitter and then using other PBS at 45°. Finally, the local unitaries on the polarization state of Bob is implemented by using

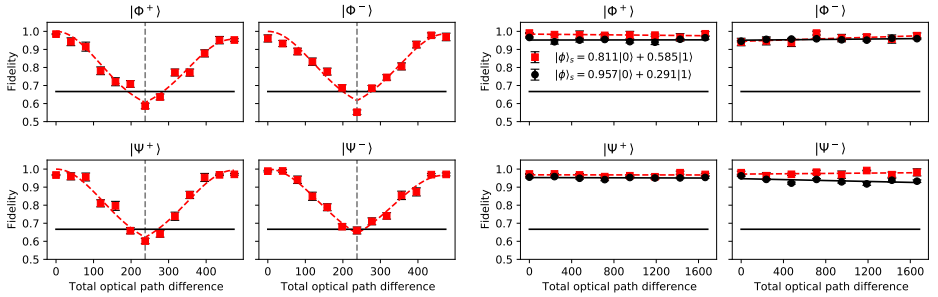

Figure 3.6: The teleportation fidelity including the error bars as a function of the interaction time, denoted by the total optical path difference with the unit of 808nm. On the left panel, the experimental results regarding the first case discussed in the main text are presented when Alice's state is prepared as $|\phi\rangle_s = 0.811\,|0\rangle + 0.585\,|1\rangle$. On the right panel, we plotted the results of the second experimental situation. The dashed red lines are the theoretical fit, and the black horizontal line indicates the classical limit of the fidelity with value of 2/3.

half wave plates (HWP).

We performed the experiment for all of the four outcomes of the Bell-state measurement and considering two scenarios. In the first case, we begin with realizing that increasing the noise on the side of Alice without adding any noise on the side of Bob decreases the teleporting fidelity, given by ${}_s\langle\phi|\rho_b|\phi\rangle_s$. We increase the noise till the maximum optical path difference $235.6\lambda_0$ with $\lambda_0 = 808$nm is reached. The achieved fidelity of the teleported state in the experiment is plotted in the left panel of Fig. 3.6 as a function of the optical path difference and considering $|\phi\rangle_s = 0.811\,|0\rangle + 0.585\,|1\rangle$. As we expected, the fidelity goes down by increasing the noise and crosses the classical limit of 2/3. Then after fixing the noise on Alice's side at its maximum, we start to add noise also on the Bob's side and increase it till reaching the exact amount of noise on the Alice's side. As we observe in the second half (denoted by the vertical dashed lines) of the plots in the left panel of Fig. 3.6, the fidelity starts to revive and eventually reaches some high values (for example 0.969 ± 0.021 for $|\Phi^-\rangle$) when both sides have the same amount of noise.

In the second case, we add noise to the both sides in a stepwise manner

and with the same amount. The experimental results are given in the right panel of Fig. 3.6. When there is the same amount of noise on the two sides, the fidelity does not decrease and remains basically constant. Even though the initial polarization entanglement is destroyed due to high amount of noise, this is a proof of principle experiment showing that one can achieve high-fidelity teleportation when exploiting useful resources available in the other degrees of freedom of an open quantum system.

Chapter 4

Open system dynamics as a tool in quantum thermodynamics

In this chapter, we utilize dynamics of open quantum systems to examine thermodynamic properties of the systems under scrutiny. We focus on two main goals. Firstly, we present a simple model which allows for controlling the non-Markovianity of the open dynamics. We derive the master equation for this model and discuss the relation between the degree of non-Markovianity of the dynamics and the ability of performing work by the external drive. The corresponding results are presented in Section 4.1. Secondly, we introduce a model for implementing a quantum Stirling cycle and use it as a heat engine. We derive the master equation that allows to calculate the real-time dynamics of a driven working substance in contact with a heat bath and we use it to study thermodynamic performance of the heat engine operated at finite times. These results are summarized in Section 4.2.

4.1 Open system dynamics and thermodynamics in a system of coupled two-level systems

4.1.1 The two-qubit model

We present a simple model that allows for non-Markovian dynamics. The model consists of a system of two coupled qubits, denoted by Q_1 and Q_2, with Q_2 weakly coupled to a Markovian reservoir. While Q_1 makes the

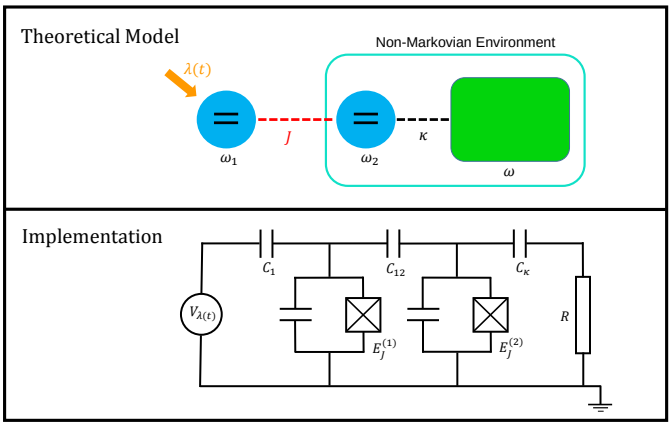

Figure 4.1: A simple model for implementing non-Markovian dynamics, shown in the upper panel, and a potential experimental setup based on superconducting qubits depicted in the lower panel. Here the resistor R plays the role of the environment and the capacitors, denoted by C, couple the superconducting qubits.

open system of interest, its effective non-Markovian environment is made of the combined system of Q_2 and the Markovian reservoir, such that the second qubit is the part of the environment keeping the memory. Moreover, we allow for coherent weak driving of Q_1 by an external field. Therefore, energy is pumped into the first qubit in the form of work and then from the second qubit dissipates into the environment (heat bath) in the form of heat. The theoretical model and a potential implementation based on superconducting qubits are illustrated in Fig. 4.1.

The total Hamiltonian of the two-qubit system and the heat bath is given by

$$\begin{aligned} \mathrm{H}(t) = &\sum_{j=1}^{2} \frac{\omega_j}{2}\sigma_z^{(j)} + \sum_{\omega} \omega b_\omega^\dagger b_\omega + J\sigma_x^{(1)}\sigma_x^{(2)} + \lambda(t)\sigma_x^{(1)} \\ &+ \kappa \sum_{\omega} g_\omega(\sigma_+^{(2)} b_\omega + \sigma_-^{(2)} b_\omega^\dagger), \end{aligned} \tag{4.1}$$

where $\sigma_{x,y}$ are the Pauli operators, and $\sigma_\pm$ are the inversion operators. Also ω_j is the frequency of the jth qubit, $b_\omega, b_\omega^\dagger$ are the annihilation and creation

operators of the environment mode at frequency ω, J is the coupling constant between the two qubits, $\lambda(t)$ is a time-dependent driving protocol and $g(\omega)$ is the spectral function of the environment. We specifically consider a periodic driving field acting on Q_1, such that $\lambda(t) = \lambda_0 \sin[\omega_D t]$.

Master equation

Since the bipartite system of Q_1 and Q_2 is weakly coupled to the heat bath, it is intuitive to use a Markovian master equation for the reduced dynamics of the two-qubit system. Once the density matrix of the bipartite system is obtained, one can get the reduced state of Q_1 by tracing over the second qubit. To make things much simpler, we restrict ourselves to a weak driving of Q_1, such that the change in the energy levels of the bipartite system due to the external drive is small. In that case, we can ignore the effect of the drive in the dissipator of the master equation. We use specifically a phenomenological master equation of the form

$$\frac{d}{dt}\rho_{12}(t) = -i[\mathrm{H}_{12}(t), \rho_{12}(t)] + \gamma^{(\downarrow)}\Big(\sigma_-^{(2)}\rho(t)\sigma_+^{(2)} - \frac{1}{2}\{\sigma_+^{(2)}\sigma_-^{(2)}, \rho_{12}(t)\}\Big) + \gamma^{(\uparrow)}\Big(\sigma_+^{(2)}\rho_{12}(t)\sigma_-^{(2)} - \frac{1}{2}\{\sigma_-^{(2)}\sigma_+^{(2)}, \rho(t)\}\Big), \tag{4.2}$$

in which $\gamma^{(\downarrow)} = (\bar{\kappa}/2)\omega_2[1 + \coth(\omega_2\beta/2)] = \gamma^{(\uparrow)}e^{\beta\omega_2}$ with $\bar{\kappa} = \kappa^2\omega_2$ are decay rates of the second qubit. Note that the accuracy of this master equation decreases by increasing the value of J, as a strong qubit-qubit interaction would influence the energy structure of the second qubit as seen by the bath. Accordingly, in addition to the restriction on the strength of the driving field, we also avoid strong qubit-qubit interactions.

For a stronger coupling, however, a microscopic derivation for the master equation should take the whole two-qubit system as the effective open system. Consequently, such a master equation would involve non-local transition operators acting on the two-qubit system, and not only Q_2. Let us partition the total Hamiltonian in Eq. (4.1) as $\mathrm{H}(t) = \mathrm{H}_S + \mathrm{H}_D(t) + \mathrm{H}_B + \mathrm{H}_I$, where we define $\mathrm{H}_S = \sum_{j=1}^{2} \frac{\omega_j}{2}\sigma_z^{(j)} + J\sigma_x^{(1)}\sigma_x^{(2)}$, $\mathrm{H}_B = \sum_\omega \omega b_\omega^\dagger b_\omega$, and $\mathrm{H}_D(t) = \lambda(t)\sigma_x^{(1)}$. Following a standard derivation based on Born and Markov approximations and up to the second order in the interaction

Hamiltonian [29], one gets

$$\frac{d}{dt}\tilde{\rho_{12}}(t) = -i[\tilde{\mathrm{H}}_D(t), \tilde{\rho_{12}}(t)] - \int_0^\infty ds \mathrm{tr}_B\Big\{[\tilde{\mathrm{H}}_I(t), [\tilde{\mathrm{H}}_I(t-s), \tilde{\rho_{12}}(t) \otimes \rho_B]]\Big\}, \tag{4.3}$$

where tilde denotes the interaction picture w.r.t. the free Hamiltonian of the two-qubit system and the bath, i.e., $\tilde{A}(t) := e^{it(\mathrm{H}_S+\mathrm{H}_B)} A e^{-it(\mathrm{H}_S+\mathrm{H}_B)}$. To recast the master equation above in a Lindblad form, the secular approximation should be applied. The spectral decomposition of the two-qubit free Hamiltonian is given by $\mathrm{H}_S = \sum_{i=1}^4 E_i \left|E_i\right\rangle \left\langle E_i\right|$, with $E_1 = -E_4 = \sqrt{J^2 + \Omega^2/4}$ and $E_2 = -E_3 = \sqrt{J^2 + \Delta^2/4}$, where we used $\Omega = \omega_1 + \omega_2$ and $\Delta = \omega_1 - \omega_2$. Thus, the bipartite system is subjected to two different transitions with frequencies $\epsilon_1 = E_4 - E_3 = E_2 - E_1$ and $\epsilon_2 = E_4 - E_2 = E_3 - E_1$. The secular approximation requires that $|\epsilon_1 - \epsilon_2|^{-1} \ll \tau_R$, where τ_R is the relaxation time of the open system. This requirement restricts the value of J and Δ. For example, for resonant qubits ($\Delta = 0$) the secular approximation may fail when J is comparable to the coupling to the bath. In this case, the master equation can not be recast in the Lindblad form. Nonetheless, the phenomenological master equation given in Eq. (4.2) seems reliable in that regime, as in the limit of $J \to 0$ the dissipator must act only on the second qubit. It is worth also mentioning that if we decompose Eq. (4.2) w.r.t. to the non-local transition operators of the two-qubit system, one finds that the phenomenological master equation contains both rotating and counter rotating terms.

4.1.2 Non-Markovianity of the dynamics

Although the dynamics of the two-qubit system is always Markovian in our setting, the reduced dynamics of the first qubit might be non-Markovian due the interaction with the second qubit. When $J \to 0$ the two qubits disconnect and Q_1 is basically isolated from the bath. For a non-zero value of J the first qubit interacts with the bath indirectly through the second qubit. A natural question would be to ask what is the smallest value of the ratio $J/\bar{\kappa}$ with which non-Markovianity kicks in. To answer to this question we consider the undriven system, in order to rule out any effect of the drive on the dynamics. Reduced dynamics of Q_1 then can be obtained by having its state $\rho_1(t) = \mathrm{tr}_2[\rho_{12}(t)]$ at all times $t \geq 0$, considering that the two-qubit state $\rho_{12}(t)$ can be achieved by solving the master equation

in Eq. (4.2).

To capture non-Markovianity in the dynamics of Q_1 we use the approach based on the volume of accessible states [67]. This method provides us a computationally simple way to explore the relation between the non-Markovianity of the system and the qubit-qubit coupling strength J. Consider the evolution of the Bloch vector of the first qubit's state governed by a transformation matrix A plus a possible translation T, such that $\vec{r}(t) = A(t)\vec{r}(0) + \vec{T}(t)$. As we discussed in Chapter 2, any temporal increase in the determinant of the transformation matrix A is a witness of non-Markovianity. We plot $|A(t)|$ as a function of the interaction time and for different values of the ratio $J/\bar{\kappa}$ in Fig. 4.2 considering resonant and non-resonant qubits. As expected, non-monotonic behavior appears in the volume of accessible states as we increase $J/\bar{\kappa}$. There is a slight difference between resonant and non-resonant cases though. Intuitively, when the qubits are resonant the first qubit is effectively coupled to the Markovian bath, thus a larger value of $J/\bar{\kappa}$ is required to observe non-Markovianity. The other parameter playing a role in the transition from Markovian to non-Markovian dynamics is the temperature of the bath. Let us describe the smallest value of $J/\bar{\kappa}$ for which the volume of accessible states behaves non-monotonically by $(J/\bar{\kappa})_{th}$. In Fig. 4.3 we have plotted the value of $(J/\bar{\kappa})_{th}$ as a function of the inverse temperature of the bath. As we expected the detuned setting comes with a higher value of $(J/\bar{\kappa})_{th}$ for most of the temperature range. We also observe that the threshold value of J increases as the bath gets warmer, as expected.

4.1.3 The average work done on the system

An active research topic is to address whether non-Markovianity of the dynamics can be used as a resource in quantum thermodynamics, for example see [39, 97–99]. In this spirit we investigate if non-Markovianity of the dynamics and the ability to perform work on the working substance are related. The simple model we introduced here allows us to control the extent of non-Markovianity by changing the coupling strength J. Thus, having the work done on the first qubit allows us to shed some light on this matter.

The average work done by the external drive on the two-qubit system

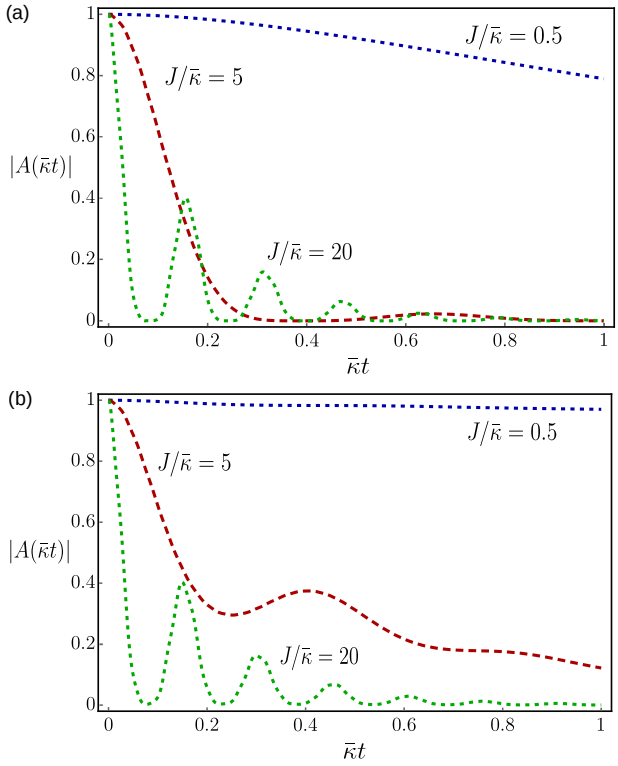

Figure 4.2: Temporal behavior of $|A(t)|$ for three different values of $J/\bar{\kappa}$. In the panel (a) qubits are resonant, $\Delta/\bar{\kappa} = 0$, while in the panel (b) we set $\Delta/\bar{\kappa} = 11$. In both of the panels we set $\omega_2\beta = 0.35$ and $\bar{\kappa} = 0.01$.

in the interval $[0, t]$ is given by

$$\langle W(t)\rangle_{12} = \int_0^t ds\ \mathrm{tr}_{12}[\dot{\mathrm{H}}_D(s)\rho_{12}(s)]. \tag{4.4}$$

Since H_D is a local operator acting only on the first qubit, the expression above also gives the average work done on the first qubit. For a periodic driving protocol as $\mathrm{H}_D(t) = \lambda_0 \sin(\omega_D t)$, the average work is consequently dependent on the frequency ω_D. A relevant question here is whether setting ω_D in resonance with the first qubit as a distinct entity or consider the level structure of the two qubit system. In Fig. 4.4, we take into account both

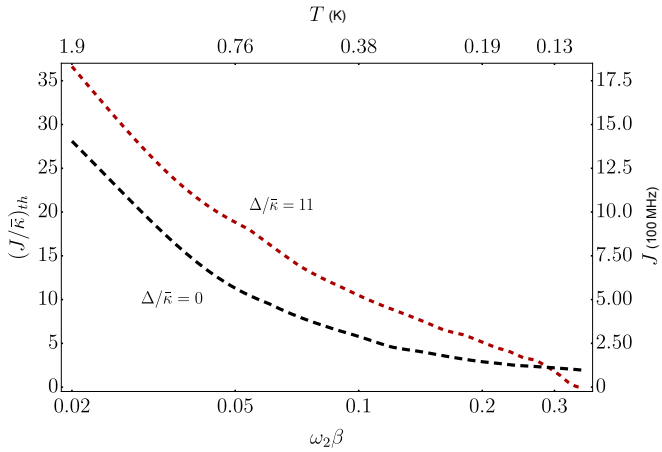

Figure 4.3: Threshold value of J for Markovian to non-Markovian crossover denoted by $(J/\bar{k})_{th}$ versus temperature of the Markovian bath (in *log* scale). The large-dashed black line corresponds to the resonant case, while the small-dashed red line presents the non-resonant case with $\Delta/\bar{k} = 11$.

cases by setting $\omega_D = \omega_1$ and $\omega_D = \epsilon_1$. The average work done on the system is plotted as a function of interaction time. The bold feature regarding both cases here is a suppression (damping of the oscillations) of the average work when the dynamics moves from Markovian to non-Markovian regime (due to increasing the value of $J/\bar{\kappa}$). Because of the sinusoidal driving the average work shows oscillations which are damped due to the interaction with the bath. This behavior is apparent for small values of $J/\bar{\kappa}$ at which the dynamics is Markovian. However, for stronger values of qubit-qubit coupling (blue and green lines) the average work does not show the same behavior. This effect is more enhanced in the case of bare-frequency driving (upper panel). One may interpret this suppression as the consequence of out of resonance driving – due to the fact that the driving frequency is fixed but the energy levels are influenced by J. However, the same behavior also exists for $\omega_D = \epsilon_1$, where the driving frequency is also J-dependent. At longer times, the system reaches a time-dependent steady state and the average work changes linearly in time.

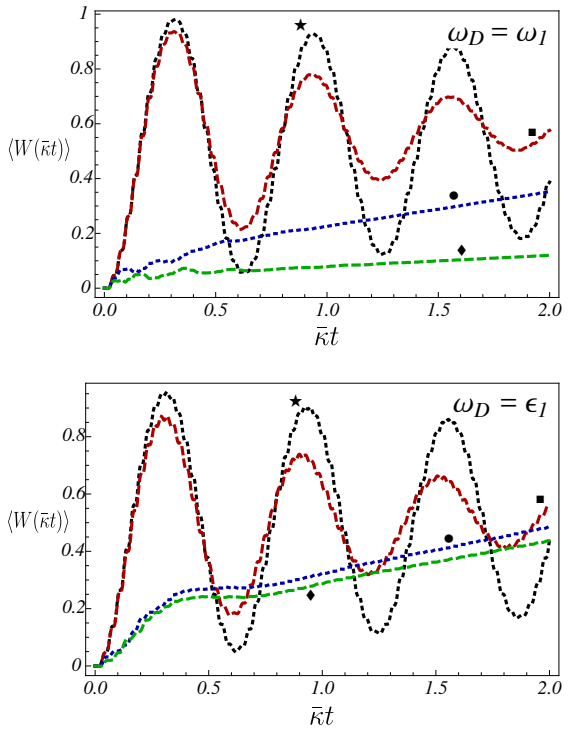

Figure 4.4: The average work performed on Q_1 considering $\omega_2\beta = 0.2$, $\Delta/\bar{\kappa} = 0$ and for $J/\bar{\kappa} = 1$ (dotted black marked by star), 2 (dashed red marked by square), 20 (dotted blue marked by circle), 30 (dashed green marked by diamond). In the lower panel we set $\omega_D = \epsilon_1$ while in the upper panel $\omega_D = \omega_1$.

4.2 Finite-time quantum Stirling heat engine

Any realistic heat engine that transfers heat to extractable work has to operate with a finite cyclic period, considering both the fact that the engine is supposed to operate in a desired finite time window and the fact that the output power goes to zero for an everlasting period. However, we also know that reversible thermodynamic processes that give the maximum extractable work are quasi-static. Therefore, a natural goal is to seek for a trade-off between power and efficiency in the processes performed at finite

times.

In particular, finite-time adiabatic processes and thereby finite-time Otto cycle have attracted much attention, for example in [98, 100–102]. Comparing adiabatic and isothermal processes, the latter is more difficult to handle at finite times due to the simultaneous coherent driving and non-unitary dissipation. Consequently, a slow drive is usually assumed when the working substance is connected to the bath, such that the non-adiabatic effects of the drive on the dissipator can be ignored. Provided that the time scales of the external drive and those of the coupling to the bath are separated, non-adiabatic effects can also be addressed using a time-dependent Markovian master equation [103].

In this part of the thesis, we study the real-time open dynamics of a driven qubit coupled to a heat bath. For this aim, a non-Markovian master equation is employed which does not assume a separation of the time scales involved in the dynamics [104, 105]. We use this tool specifically in studying performance of a finite-time quantum Stirling heat engine.

4.2.1 Physical model and open system dynamics

The Stirling cycle

As we discussed earlier, the Stirling cycle contains two isothermal strokes and two isochoric thermalization strokes. In classical settings, isochoric strokes usually involve the interaction of the working substance with a so-called regenerator. However, the model considered here does not include a regenerative setting, instead, we assume a direct interaction of the working substance with the heat baths. Inverse temperature versus level separation and polarization versus level separation diagrams for the quasistatic cycle are depicted respectively in the panels (a) and (b) of Fig. 4.5, where polarization is defined as $n(t) = \mathrm{tr}[\mathrm{H}_S(t)\rho(t)]/\omega(t)$. We discussed the four strokes of the ideally slow cycle in section 2.4. Note that however, the situation here can be different as the term *isothermal* refers now to the open system dynamics of a driven system in contact with a bath at constant temperature. One should note that the actual trajectory of the working substance can be away from the manifold of the equilibrium states due to the finite-time driving. By denoting the duration of each stroke by τ_{ij}, the period of a full cycle is $T = \tau_{ab} + \tau_{bc} + \tau_{cd} + \tau_{da}$.

To implement the Stirling cycle we suggest using a superconducting

circuit, schematically shown in the panel (e) of Fig. 4.5, which has been also suggested as a possible implementation of the Otto refrigerator [101]. The free Hamiltonian of the qubit and its coupling to the hot/cold bath are respectively denoted by $\mathrm{H}_S(t)$ and $\mathrm{H}_I^{(h/c)}(t)$ and are given by ($\hbar = 1$)

$$\mathrm{H}_S(t) = \omega_0[q(t)\sigma_z + \Delta\sigma_x], \quad \mathrm{H}_I^{(\alpha)}(t) = \lambda_\alpha(t)\sigma_y \otimes \mathrm{B}_\alpha, \tag{4.5}$$

where ω_0 denotes a reference energy scale for the non-driven qubit. The operator B_α acts on the bath with $\alpha = c, h$ denoting the cold and the hot baths. Moreover, $\lambda_\alpha(t)$ is a piece-wise continuous function which is used to switch the coupling between the two baths, as shown in the panel (d) of Fig. 4.5. We note that, to implement the switching of the interaction between the qubit and the baths at steps b and d in the cycle, a tunable coupler is required. This can be realized, for example, by using an extra qubit or a resonator between the main qubit and the baths and tuning the corresponding frequencies in resonance or out of resonance. For the sake of simplicity, however, we do not take into account a detailed physical model for the coupler and instead assume an ideal case which can be given by a piece-wise continuous function. As depicted in the panel (d) of Fig. 4.5, we choose the driving protocol $q(t)$ such that the instantaneous level separation of the qubit, denoted by $\omega(t) = 2\omega_0\sqrt{q(t)^2 + \Delta^2}$, changes linearly within the interval $[\omega_1, \omega_2]$ with a given fixed speed. One finds accordingly $q(t) = \sqrt{\omega(t)^2/4 - \Delta^2}$. Moreover, the coupling spectrum of the bath is given by $G(\omega) = \int_{-\infty}^{+\infty} ds e^{i\omega s}\langle \mathrm{B}(s)\mathrm{B}\rangle$. A relevant expression for the coupling spectrum regarding the aforementioned setup is shown in the panel (c) of Fig. 4.5 and is given by [101, 106]

$$G_{\beta,g_i}(\omega \geq 0) \quad = \quad \frac{g_i^2}{1 + f_i^2(\frac{\omega}{\omega_i} - \frac{\omega_i}{\omega})^2} \times \frac{\omega}{1 - e^{-\beta\omega}}, \tag{4.6}$$

where $i = c, h$ refers to the quantities of the cold and hot baths, g_i denotes the coupling strength, $\omega_i = 1/\sqrt{L_i C_i}$ gives resonance frequency of the baths, and $f_i = R_i^{-1}/\sqrt{L_i/C_i}$ is the quality factor of the bath's resonator [101]. We also have the relation $G_{\beta,g}(-\omega) = e^{-\beta\omega}G_{\beta,g}(\omega)$. Here, we assume that the two baths have the same quality factor f and also the same resonance frequency ω_r. In addition, values of the coupling strengths g_c and g_h are set such that the corresponding spectra have the same amplitudes at ω_r (see panel (c) of Fig. 4.5).

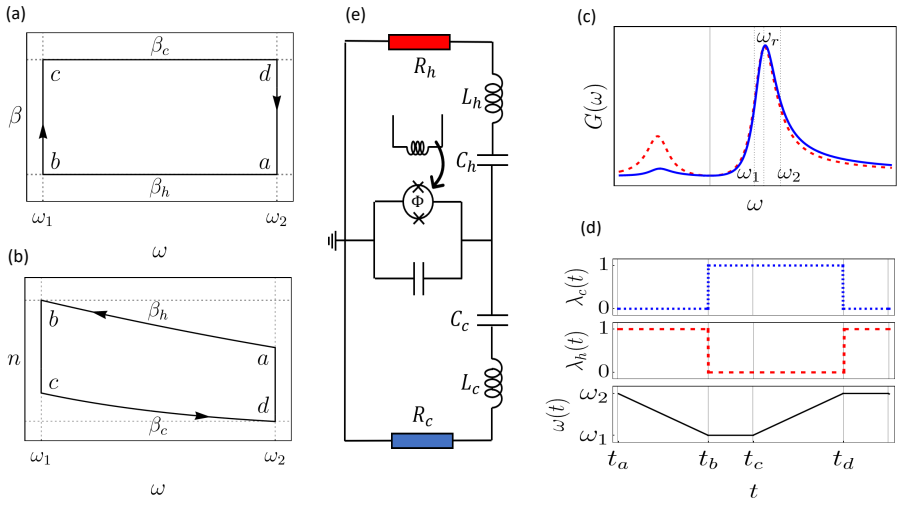

Figure 4.5: The quantum Stirling cycle used as a heat engine and its implementation using superconducting circuits. The temperature and the polarization versus the level separation diagrams of the ideally slow cycle shown in the panel (a) and the panel (b). Panel (c) shows the coupling spectra of the two heat baths. Panel (d) shows the time-dependent coupling to the heat baths and the linear driving of the two-level system as a function of time. In the panel (e) we propose an implementation of the cycle by a superconducting qubit that is capacitively coupled to two RLC circuits (including the resistors R_i, inductors L_i, and capacitors C_i), playing the role of the cold and hot baths. External driving is done by changing the magnetic flux over the qubit.

Dynamics

To obtain the real-time dynamics of the driven qubit in contact with the heat bath, a general non-Markovian master equation has been derived based on the Nakajima-Zwanzig method and assuming weak coupling and Born approximations [104, 105]. This master equation does not require a separation of the time scales of the drive and those of the baths and it includes both rotating and counter-rotating contributions.

We first briefly introduce the master equation and discuss its general form. Consider a driven qubit in contact with a thermal bath at an inverse

temperature β. The total Hamiltonian of the system reads

$$\mathrm{H}(t) = \mathrm{H}_S(t) + \mathrm{H}_I(t) + \mathrm{H}_B, \tag{4.7}$$

where $\mathrm{H}_S(t)$ and $\mathrm{H}_B(t)$ are the free Hamiltonian of the open system and the bath respectively. By writing the interaction Hamiltonian as $\mathrm{H}_I(t) = \mathrm{S}(t) \otimes \mathrm{B}$ the master equation reads [104, 105]

$$\mathcal{L}_t[\rho(t)] = -i[\mathrm{H}_S(t), \rho(t)] + \int_0^t d\tau \ \left[\Phi(t-\tau)[\tilde{\mathrm{S}}(t,\tau)\rho(t), \mathrm{S}(t)] + \mathrm{h.c}\right], \tag{4.8}$$

where

$$\tilde{\mathrm{S}}(t,\tau) = \mathrm{U}(t,\tau)\mathrm{S}(\tau)\mathrm{U}(t,\tau)^\dagger, \tag{4.9}$$

$$\mathrm{U}(t,\tau) = \mathcal{T}_+ e^{-i\int_\tau^t ds \mathrm{H}_S(s)}, \tag{4.10}$$

$$\Phi(t) = \langle e^{i\mathrm{H}_B t}\mathrm{B}e^{-i\mathrm{H}_B t}\mathrm{B}\rangle. \tag{4.11}$$

The key to solve the master equation above is to obtain a solution for the unitary propagator $\mathrm{U}(t,\tau)$. In general this can be handled numerically, specifically when the system's Hamiltonian does not commute with itself at different times. Also note that the contribution of two different baths are additive by construction if one assumes that the baths are initially uncorrelated, as we consider in this thesis.

Now we consider the specific system given by the total Hamiltonian in Eq. (4.5). To have more intuition about the operatorial form of the master equation, let us decompose all the operators in the master equation w.r.t. the instantaneous eigenvectors of $\mathrm{H}_S(t)$ given by

$$\begin{aligned} |\epsilon_e(t)\rangle &= \cos\theta_t |e\rangle + \sin\theta_t |g\rangle, \\ |\epsilon_g(t)\rangle &= \sin\theta_t |e\rangle - \cos\theta_t |g\rangle, \end{aligned} \tag{4.12}$$

with $\theta_t = (1/2)\cot^{-1}(q(t)/\Delta)$ and $|e(g)\rangle$ as the eigenbasis of σ_z. By defining the transition operator $\mathrm{L}(t) = |\epsilon_g(t)\rangle\langle\epsilon_e(t)|$ between the instantaneous energy basis of the qubit, the master equation contains a rotating and a

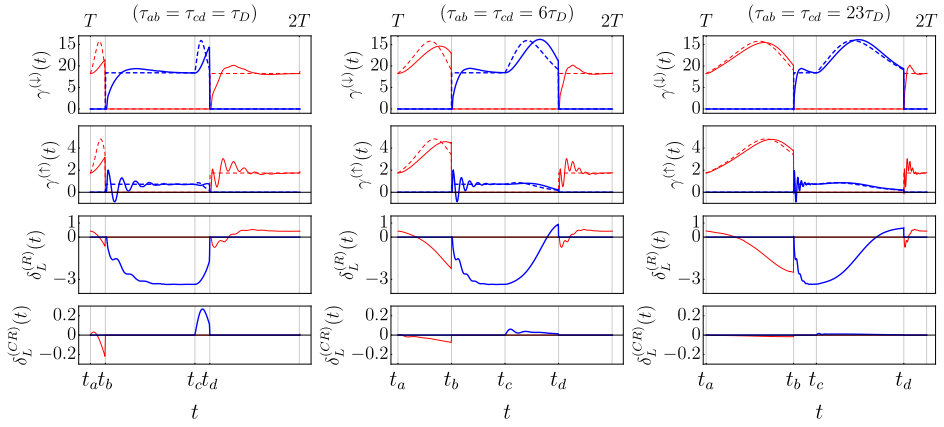

Figure 4.6: Numerical values of the transition rates (in the unit of 10^{-2}) as a function of time for three different driving speeds denoted in the title of each plot. The two upper rows show the instantaneous transition rates plotted in solid curves, while the dashed lines are their asymptotic Markovian limit $2\pi G(\pm\omega(t))$. The two lower rows depict the rotating and counter-rotating Lamb shift contributions as a function of time.

counter-rotating part and takes the explicit form

$$\begin{aligned}\mathcal{L}_t[\rho(t)] = &-i\left[\left(1+\delta_L^{(R)}(t)\right)\mathrm{H}_S(t) + \delta_L^{(CR)}(t)\left(\Delta\sigma_z - q(t)\sigma_x\right), \rho(t)\right] \\ &+\gamma^{(\downarrow)}(t)\left[\mathrm{L}(t)\rho(t)\mathrm{L}^\dagger(t) - \frac{1}{2}\{\mathrm{L}^\dagger(t)\mathrm{L}(t), \rho(t)\}\right] \\ &+\gamma^{(\uparrow)}(t)\left[\mathrm{L}^\dagger(t)\rho(t)\mathrm{L}(t) - \frac{1}{2}\{\mathrm{L}(t)\mathrm{L}^\dagger(t), \rho(t)\}\right] + \mathcal{D}_t^{(CR)}[\rho(t)],\end{aligned} \tag{4.13}$$

Here $\delta^{(R/CR)}$ are the bath-induced rotating/counter-rotating Lamb shifts, $\gamma^{(\downarrow/\uparrow)}(t)$ are the transition rates in the rotating part of the dissipator and $\mathcal{D}_t^{(CR)}$ is the counter-rotating part of the dissipator. Note that, the rotating Lamb shift is proportional to $\mathrm{H}_S(t)$, but the counter-rotating contribution does not commute with the free Hamiltonian of the qubit. We set the duration of the isochoric strokes fixed and study the temporal behavior of the transition rates during the isothermal strokes by changing the speed of compression and expansion ramping. The numerically calculated

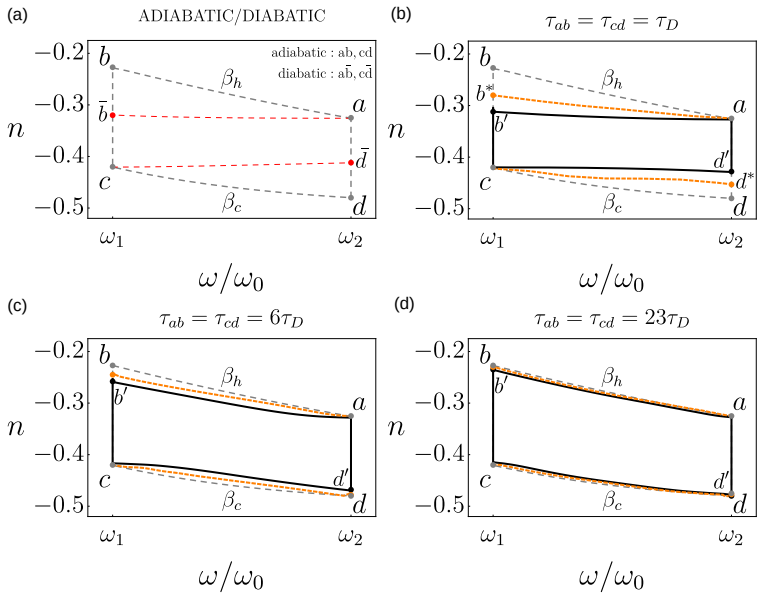

Figure 4.7: Polarization versus level separation diagram for different driving speeds. In panel (a) the ideal slow cycle follows the adiabatic trajectories ab and cd, whereas the diabatic trajectories are depicted by $a\bar{b}$ and $c\bar{d}$. Trajectories for three different values of the finite-time compression and expansion speeds are shown by ab' and cd' in the rest of the panels.

rates are plotted in Fig. 4.6. The rates $\gamma^{(\downarrow/\uparrow)}$ approach their Markovian limit $2\pi G(\pm\omega(t))$, plotted using the dashed lines, when the duration of the isothermal strokes is large. For the faster processes, however, one notices a deviation of the rates from the Markovian limit.

Two asymptotic cases can be considered: (1) adiabatic slow driving leading to an ideal isothermal trajectory and (2) diabatic driving which is so fast that the state of the qubit does not have time to change its configuration at all. In the first case the process is quasistatic, allowing the state of the qubit to maintain its equilibrium configuration during the process. For example, for the processes $a \to b$ one would have $\rho(t) = e^{i\mathrm{H}_S(t)\beta}/\mathrm{tr}[e^{i\mathrm{H}_S(t)\beta}]$ with $t \in [t_a, t_b]$. On the other hand, when the process is diabatic the state of the qubit does not change and holds its initial configuration, i.e., $\rho(t) = e^{i\mathrm{H}_S(t_a)\beta}/\mathrm{tr}[e^{i\mathrm{H}_S(t_a)\beta}]$ with $t \in [t_a, t_b]$. In this work, we set the duration of

the isochoric strokes long enough to let the qubit reach equilibrium with the baths at the end points a and c. Thus, these two points are always fixed in our analysis. Accordingly, the adiabatic and diabatic are shown in the panel (a) of Fig. 4.7, with the trajectories $a \to b$ and $c \to d$ denoting the ideal isothermal processes while $a \to \bar{b}$ and $c \to \bar{d}$ representing the diabatic limit. One expects that the finite-time processes will lead to trajectories that are confined within the $a\bar{b}b$ and $c\bar{d}d$ triangles. We label the trajectory of a finite-time cycle by $ab'cd'a$. Thus, at the end of the compression and expansion processes, the qubit will end up at the points b' and d', instead of b and d. In the other panels of Fig. 4.7, we plot the real-time trajectories of the qubit dynamics (black solid curves) for different speeds of driving. The dashed orange curves correspond to the instantaneous steady state of the qubit. The latter is obtained by fixing the generator of Eq. (4.13) at its configuration at a given time t and then letting the dynamics continue till reaching a steady state, which we label by ρ_t^*. Accordingly, the end points corresponding to $\rho_{t_b}^*$ and $\rho_{t_d}^*$ are labeled respectively by b^* and d^*.

4.2.2 Performance of the heat engine running in the finite times

Our main goal is to investigate the possible advantages in the performance of the heat engine when changing the driving speed, thereby changing the trajectory $ab'cd'a$ between the adiabatic and diabatic limits. Specifically, we can seek for enhancement in the output power or in the efficiency comparing to the adiabatic cycle $abcda$.

Before presenting the main results, let us clarify some points. Firstly, note that, due to the time-dependency of the rates, we need to set $t_a = T$ and exclude the first cycle with $0 \leq t < T$. This guarantees that the generator of the dynamics and the state of the qubit both reset to their initial configurations at $t = 2T$. Secondly, since the cycle is not a regenerative one and the qubit directly interacts with the baths, the net heat absorbed during a full cycle includes contributions from both the processes $a \to b'$ and $d' \to a$. Thirdly, the presence of Lamb shifts has some non-trivial consequences. In particular, the work done on the qubit may have a part coming from the time-dependent Lamb shifts, in addition to the external drive as the main source.

We consider first identical speed of compression and expansion processes, i.e., $\tau_{ab} = \tau_{cd}$. Efficiency is plotted as a function of $\tau_{ab,cd}$ using

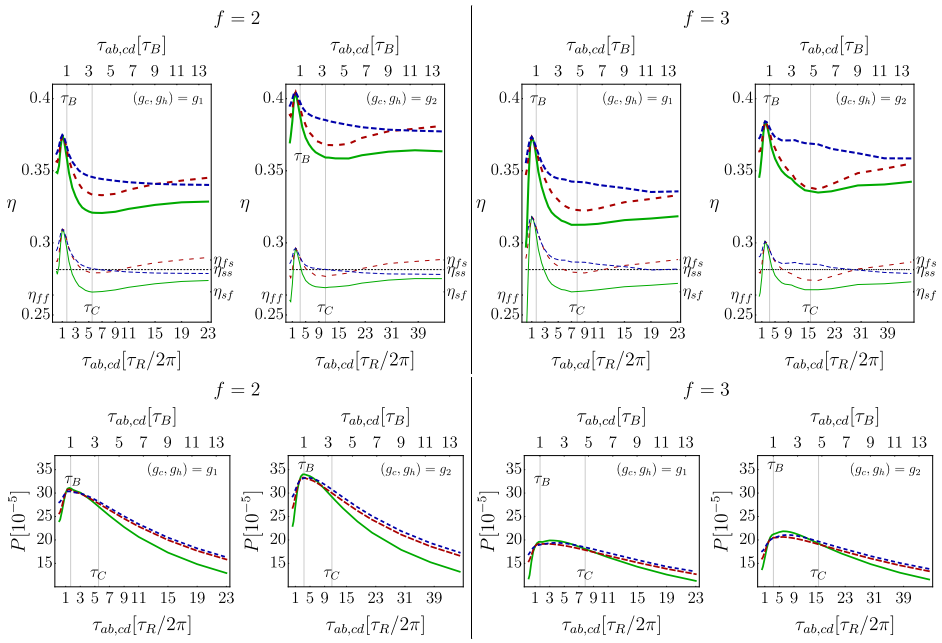

Figure 4.8: The efficiency and the output power as a function of driving speed for different values of the relaxation/correlation time. The relaxation time is twice when considering the coupling strengths denoted by g_1. In the plots of efficiency, the solid curves correspond to the symmetric driving with $\tau_{ab} = \tau_{cd}$. The asymmetric cases are shown using the large dashing red and the small dashing blue lines, corresponding respectively to (1) τ_{ab} being fixed and (2): τ_{cd} being fixed. In the upper panel, the thick curves correspond to the effective Hamiltonian and the thin lines to the free Hamiltonian. The power is calculated using the free Hamiltonian. The dashed black horizontal line shows the analytic value of the efficiency of the asymptotic slow (adiabatic) cycle, denoted by η_{ss}. Also, $\eta_{sf(fs)}$ is the analytic value of efficiency for adiabatic(diabatic) compression followed by diabatic(adiabatic) expansion.

the solid curves in the upper panel of Fig. 4.8, where we did the calculations considering both the effective Hamiltonian that includes the Lamb shifts (thick green curves) and the free Hamiltonian (thin green curves). An interesting result is a peak that exceeds the efficiency of the adiabatic cycle *abcda*. The relevant question is now what is the relation between the observed efficiency enhancement and different time scales involved in the dynamics of the qubit, e.g., the relaxation time τ_R, bath correlation time τ_C, and bath resonance time scale τ_B. To understand this, we have plotted the efficiency considering two different values of the relaxation time (one being twice the other), and two different values of the correlation time (with the ratio 1.43), which are set by choosing $f = 2$ and $f = 3$. Moreover, we keep the value of τ_B fixed for all the four mentioned cases. Looking at Fig. 4.8, it is clear that the relevant parameter for the observed peak is the bath resonance time τ_B, such that the efficiency boosts when $\tau_{ab(cd)}$ are close to τ_B. On the contrary, it seems that when the time scale of the drive is close to the bath correlation time τ_C the efficiency decreases.

Let us now turn our attention to output power. We calculate the power by using the free Hamiltonian $\mathrm{H}_S(t)$ and exclude the Lamb shifts. The output power of the cycle for the same settings as discussed for the efficiency are plotted in the lower panel of Fig. 4.8. Interestingly, the average output power benefits from enhancement when $\tau_{ab,cd} \simeq \tau_B$ too, although the peak in the power comes at a slightly larger time scale than those for the efficiency. As expected, the output power decreases by increasing the duration of processes. The same thing also holds for very fast driving situations because the extractable work diminishes due to the higher extent of irreversibility in the processes.

The average heat transferred, the average work and the net average work are plotted in Fig. 4.9 considering the effective Hamiltonian in the left panel, and the free Hamiltonian in the right panel. Using the effective Hamiltonian to calculate the energy terms leads to some non-zero amount of average work for the isochoric strokes due to the time-dependent Lamb shifts. In addition, the average work in the $c \to d'$ is higher when considering the effective Hamiltonian. This is also due to the non-zero Lamb shift which leads to a larger effective frequency span than $\Delta\omega = \omega_2 - \omega_1$. As we expected, the average net work approaches its adiabatic limit as we increase $\tau_{ab,cd}$ and decreases by speeding up the drive. Moreover, by speeding up the processes, the qubit has less and less time to interact with the baths. This results in the vanishing heat transferred at fast driving. Finally it is worth

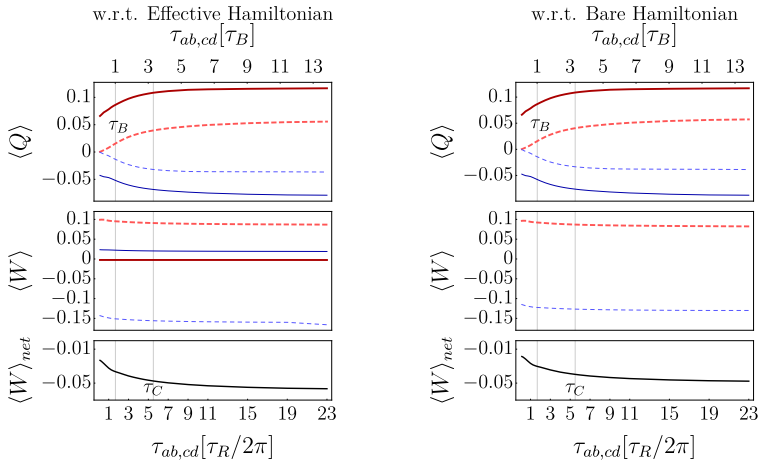

Figure 4.9: The average heat, the average work and the net average work as a function of the driving duration considering both the free Hamiltonian and the effective Hamiltonian. In the plots of the average heat and the average work, the thick dashed red curves correspond to the $a \to b$ process, the thin solid blue curves to the $b \to c$ process, the thin dashed blue to the $c \to d$ process and the thick red curve to $d \to a$ process.

mentioning that the heat transferred during the isochoric strokes reaches its non-zero minimum by approaching the diabatic limit (points $\bar{b}$ and $\bar{d}$ in Fig. 4.7).

Besides these asymptotic scenarios, we see a dip in the heat transferred and the net average work at some scale of $\tau_{ab,cd}$ matching with the peak in the efficiency. This basically indicates suppression of the heat transferred to the cold bath. If the qubit dissipates less to the cold bath it means that the work done is higher and thereby the efficiency would be higher as well. This may suggest that a faster $a \to b'$ process in Fig. 4.7 would be in general beneficial, since the state at the end point b' gets closer to the equilibrium state at the point c and there would be less dissipated heat to the cold bath. Nonetheless, the faster is the $a \to b'$ process, the less heat will be absorbed from the hot bath, which in turn results in less extractable work. A similar situation also happens for the $c \to d'$ process, considering the heat dissipated during the expansion and the heat absorbed during the $d' \to a$ process. Thus, there must be some trade-off in some intermediate

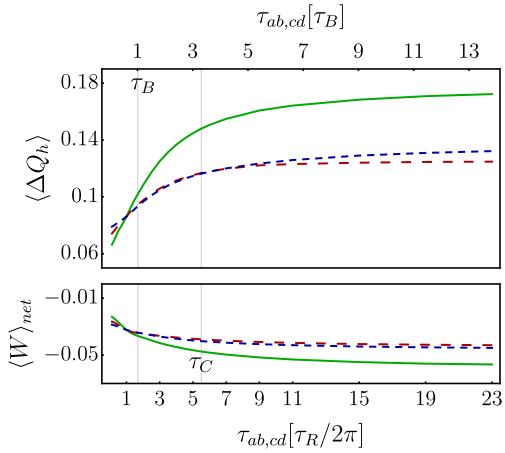

Figure 4.10: The net average work and net heat transferred as a function of driving duration. The solid green curves describe the symmetric driving scenario, the large dashed red represents the asymmetric driving case when τ_{ab} is fixed, and the small dashed blue shows the asymmetric case with τ_{cd} being fixed.

situation that provides the optimum efficiency.

A final issue we investigate is whether asymmetric speed of the compression and expansion would have some non-trivial effect on the performance of the engine. To make this clear, we analyze two different situations. In the first case we set τ_{ab} fixed while we change τ_{cd}, whereas, for the second case we fix τ_{cd} and alter τ_{ab}. The fixed values considered here are identical to the relaxation time of the qubit. The efficiency and the average output power of these cases are plotted in Fig. 4.8 by using large dashed red and small dashed blue lines, respectively. Similar to the case of symmetric driving, the thick curves correspond to calculating the energies w.r.t. the effective Hamiltonian and the thin curves to the free Hamiltonian. Interestingly, efficiency of the asymmetric cycles is always higher than the symmetric ones. Superiority of the two asymmetric cases with respect to each other depends non-trivially on the time scale of the driving though. Energy flow into and from the qubit regarding the asymmetric cycles are shown in Fig. 4.10. The net average work is dependent on the total time

of the expansion and compression processes, $\tau_{tot} = \tau_{ab} + \tau_{cd}$, such that the faster we drive the higher is the irreversibility and thus extractable work decreases. Note that, the two asymmetric cycles with the same value of τ_{tot} provide slightly different amount of the net average work. This again highlights the importance of the finite-time effects in the performance of the heat engines.

Chapter 5

Conclusions

In this thesis, we presented our results on the open dynamics of quantum systems in the framework of both new quantum information protocols and quantum thermodynamics. Conventional quantum information protocols with open systems require to control and, more importantly, to suppress decoherence. On the contrary, in this thesis the focus is on the theoretical and experimental know-how that allow us to utilize the environment to better perform the protocols. We also studied the open dynamics of driven quantum systems with the goal of finding the relations between the dynamical and thermodynamic properties of the systems.

In Chapter 2, we recalled some basic concepts of quantum theory related to the results of the thesis. Specifically, we reviewed the dynamics of quantum systems, some basic topics in quantum information theory and also a dynamical approach to quantum thermodynamics. After this introductory part, the results of the thesis were presented, depending on their relation to either quantum information or thermodynamics, in two chapters.

Chapter 3 covered the results about quantum information protocols with two-photon dephasing model, which are related to the original results of the papers I, III, and IV. After recalling the single-photon dephasing model and its implementation, we discussed two-photon polarization open dynamics and presented a related master equation approach based on the results of paper III. The master equation, derived in the Lindblad form, allowed us to investigate the role of initial frequency-frequency correlation (initial correlation within the environment) in the dynamics. We discussed how both the transition rates and the operators are dependent on the properties of the environment modeled by bivariant Gaussian distributions. We showed how the two-photon polarization open dynamics is governed by the local (at the level of single photon) or the global operators depending on

the initial correlations in the environment. Besides the local versus global nature of the open dynamics, we also discussed how initial correlations lead to non-Markovianity in the dynamics, which reflects itself in the negative transition rates of the master equation.

In the second section of Chapter 3, we concentrated on the paper I which provides a protocol to generate polarization entanglement remotely due to interference in the frequency domain. We first briefly discussed how superposing different paths of an interferometer can lead to generation of entanglement in an ancillary quantum system coupled to the interferometric degrees of freedom. For implementing this idea we proposed a protocol based on a two-photon system subjected to local dephasing and frequency up-conversion processes. In this protocol, frequency of the photon pair provides an interferometric degrees of freedom, to which we couple the two-photon polarization using local dephasing dynamics. To generate the polarization entanglement, we utilized local frequency up-conversion processes which erase the frequency distinguishability and lead to interference in the frequency domain. We showed that the key to the protocol is the initial frequency-frequency correlations that lead to non-local memory effects. These allow us to prepare the desired total polarization-frequency state and control the constructive/destructive interference for different polarization subspaces of the two-photon system. The peculiar feature of this protocol is that the required operations are local on each photon. Thus, in principle this protocol can be used to generate polarization entanglement between two distant photons.

We dedicated the third section of Chapter 3 to present the results of the paper IV. There we experimentally realized a high-fidelity quantum teleportation protocol by an open quantum system. Quantum entanglement is the resource for teleporting an unknown quantum state. Thus, the fidelity of a successful teleportation with open systems goes down as a consequence of the decoherence-induced loss of entanglement. However, it has been proposed that the non-local memory effects implemented in a two-photon dephasing model can be employed to compensate the harmful effects of noise and fulfill a perfect teleportation. We adapted these theoretical know-how in an experimental setup and realized the protocol with high fidelity. We first showed that by adding the dephasing noise on the side of Alice fidelity behaves as expected. As a proof of principle, we managed to undo the harmful effects of the noise on the Alice's side and reach high teleportation fidelities by adding controlled dephasing noise on the side of Bob when

initial frequency-frequency correlations and the non-local memory effects were employed.

The second part of the thesis contains the results related to the thermodynamics of open quantum systems, gathered in Chapter 4. In the first section of this Chapter, we summarized the results of the paper II, where we examined the relation between non-Markovianity of the dynamics and the ability to perform work on the open system. We discussed how to manipulate the open dynamics of a qubit, moving from a Markovian dynamics to a non-Markovian one, by controlling its coupling to an ancillary qubit that is weakly coupled to a Markovian reservoir. Interestingly, we showed that in the non-Markovian situation, the ability of performing work on the first qubit is suppressed in comparison to the Markovian regime.

The second section of Chapter 4 focused on addressing the finite-time driving effects in dynamics and thermodynamics of a two-level system utilized as a working substance in a quantum Stirling cycle. We specifically concentrated on a cycle working as a heat engine. The main outcome of this study was two-fold. First, we showed that different time scales related to the working substance and its coupling to the heat baths are influential in the performance of the Stirling heat engine. In fact, the efficiency and output power enjoy a boost when we drive the working substance with a time scale on resonance with the baths. Interestingly, we also discussed that to get the benefits of finite-time effects, one should in principle optimize the compressing and expanding driving protocols asymmetrically and with respect to the individual properties of the bath to which the working substance is coupled during a process.

As a conclusion, the outcomes of this thesis provide new insight into using the open dynamics of quantum systems in different areas of quantum technologies. Especially, controlling the distribution and dynamics of the quantum correlations is an important tool for quantum communication technologies. We showed that in a noisy situation using other degrees of freedom in addition to the open system of interest can be resourceful. An interesting outlook of this thesis could be to investigate different physical platforms suitable for interference-induced generation of entanglement from a practical point of view, and also the required conditions to do so in a general theoretical context from a fundamental point of view.

Bibliography

[1] W. A. Miller and J. A. Wheeler, *Delayed-Choice Experiments and Bohr's Elementary Quantum Phenomenon* (World Scientific, 1997), vol. Volume 4 of *Advanced Series in Applied Physics*, pp. 72–84.

[2] X.-s. Ma, J. Kofler, and A. Zeilinger, Rev. Mod. Phys. **88**, 015005 (2016).

[3] M. Nielsen and I. Chuang, *Quantum Computation and Quantum Information* (Cambridge University Press New York, 2010).

[4] G. Benenti, G. Casati, and G. Strini, *Principles of Quantum Computation and Information* (World Scientific, 2004).

[5] D. Deutsch and R. Jozsa, Proc. R. Soc. Lond. A **439**, 553 (1992).

[6] R. Cleve, A. Ekert, C. Macchiavello, and M. Mosca, Proc. R. Soc. Lond. A **454**, 339 (1998).

[7] P. W. Shor, in *Proceedings 35th Annual Symposium on Foundations of Computer Science* (1994).

[8] L. K. Grover, in *Proceedings of the Twenty-Eighth Annual ACM Symposium on Theory of Computing* (Association for Computing Machinery, New York, NY, USA, 1996), STOC '96, p. 212–219.

[9] S. Gulde, M. Riebe, G. P. T. Lancaster, C. Becher, J. Eschner, H. Häffner, F. Schmidt-Kaler, I. L. Chuang, and R. Blatt, Nature **421**, 48 (2003).

[10] L. M. K. Vandersypen, M. Steffen, G. Breyta, C. S. Yannoni, M. H. Sherwood, and I. L. Chuang, Nature **414**, 883 (2001).

[11] I. L. Chuang, N. Gershenfeld, and M. Kubinec, Phys. Rev. Lett. **80**, 3408 (1998).

[12] A. Einstein, B. Podolsky, and N. Rosen, Phys. Rev. **47**, 777 (1935).

[13] E. Schrödinger, Math. Proc. Cambridge Philos. Soc **31**, 555–563 (1935).

[14] C. H. Bennett, G. Brassard, C. Crépeau, R. Jozsa, A. Peres, and W. K. Wootters, Phys. Rev. Lett. **70**, 1895 (1993).

[15] D. Bouwmeester, J.-W. Pan, K. Mattle, M. Eibl, H. Weinfurter, and A. Zeilinger, Nature **390**, 575 (1997).

[16] C. H. Bennett and S. J. Wiesner, Phys. Rev. Lett. **69**, 2881 (1992).

[17] K. Mattle, H. Weinfurter, P. G. Kwiat, and A. Zeilinger, Phys. Rev. Lett. **76**, 4656 (1996).

[18] C. H. Bennett and G. Brassard., in *In Proceedings of IEEE International Conference on Computers, Systems and Signal Processing* (1984).

[19] C. H. Bennett, Phys. Rev. Lett. **68**, 3121 (1992).

[20] A. K. Ekert, Phys. Rev. Lett. **67**, 661 (1991).

[21] R. P. Feynman, Engineering and Science **23**, 22 (1960).

[22] R. P. Feynman, Int. J. Theor. Phys **21**, 467 (1982).

[23] J. Preskill, arXiv e-prints arXiv:1203.5813 (2012).

[24] J. Preskill, Quantum **2**, 79 (2018).

[25] F. Arute, K. Arya, R. Babbush, D. Bacon, J. C. Bardin, R. Barends, R. Biswas, S. Boixo, F. G. S. L. Brandao, D. A. Buell, et al., Nature **574**, 505 (2019).

[26] J.-G. Ren, P. Xu, H.-L. Yong, L. Zhang, S.-K. Liao, J. Yin, W.-Y. Liu, W.-Q. Cai, M. Yang, L. Li, et al., Nature **549**, 70 (2017).

[27] S.-K. Liao, W.-Q. Cai, J. Handsteiner, B. Liu, J. Yin, L. Zhang, D. Rauch, M. Fink, J.-G. Ren, W.-Y. Liu, et al., Phys. Rev. Lett. **120**, 030501 (2018).

[28] URL `https://quantum-computing.ibm.com/`.

[29] H.-P. Breuer and F. Petruccione, *The Theory of Open Quantum Systems* (Oxford University Press, 2007).

[30] M. A. Schlosshauer, *Decoherence and the Quantum-To-Classical Transition* (Springer Berlin Heidelberg, 2007).

[31] Á. Rivas and S. F. Huelga, *Open Quantum Systems* (Springer Berlin Heidelberg, 2012).

[32] Á. Rivas, S. F. Huelga, and M. B. Plenio, Rep. Prog. Phys. **77**, 094001 (2014).

[33] H.-P. Breuer, E.-M. Laine, J. Piilo, and B. Vacchini, Rev. Mod. Phys. **88**, 021002 (2016).

[34] L. Li, M. J. Hall, and H. M. Wiseman, Phys. Rep. **759**, 1 (2018), concepts of quantum non-Markovianity: A hierarchy.

[35] C.-F. Li, G.-C. Guo, and J. Piilo, EPL **127**, 50001 (2019).

[36] C.-F. Li, G.-C. Guo, and J. Piilo, EPL **128**, 30001 (2019).

[37] F. Benatti and R. Floreanini, eds., *Irreversible Quantum Dynamics* (Springer Berlin Heidelberg, 2003).

[38] B. M. Terhal, Rev. Mod. Phys. **87**, 307 (2015).

[39] F. Binder, L. A. Correa, C. Gogolin, J. Anders, and G. Adesso, eds., *Thermodynamics in the Quantum Regime* (Springer International Publishing, 2018).

[40] J. P. Pekola, Nature Physics **11**, 118 (2015).

[41] M. Lostaglio, Rep. Prog. Phys. **82**, 114001 (2019).

[42] M. Campisi, P. Hänggi, and P. Talkner, Rev. Mod. Phys. **83**, 771 (2011).

[43] R. Kosloff, Entropy **15**, 2100 (2013).

[44] S. Vinjanampathy and J. Anders, Contemp. Phys. **57**, 545 (2016).

[45] S. Alipour, F. Benatti, F. Bakhshinezhad, M. Afsary, S. Marcantoni, and A. T. Rezakhani, Sci. Rep. **6**, 35568 (2016).

[46] S. Marcantoni, S. Alipour, F. Benatti, R. Floreanini, and A. T. Rezakhani, Sci. Rep. **7**, 12447 (2017).

[47] R. Alicki, J. Phys. A **12**, L103 (1979).

[48] H. T. Quan, Y.-x. Liu, C. P. Sun, and F. Nori, Phys. Rev. E **76**, 031105 (2007).

[49] E.-M. Laine, H.-P. Breuer, J. Piilo, C.-F. Li, and G.-C. Guo, Phys. Rev. Lett. **108**, 210402 (2012).

[50] E.-M. Laine, H.-P. Breuer, J. Piilo, C.-F. Li, and G.-C. Guo, Phys. Rev. Lett. **111**, 229901 (2013).

[51] B.-H. Liu, D.-Y. Cao, Y.-F. Huang, C.-F. Li, G.-C. Guo, E.-M. Laine, H.-P. Breuer, and J. Piilo, Sci. Rep. **3**, 1781 (2013).

[52] B.-H. Liu, X.-M. Hu, Y.-F. Huang, C.-F. Li, G.-C. Guo, A. Karlsson, E.-M. Laine, S. Maniscalco, C. Macchiavello, and J. Piilo, EPL **114**, 10005 (2016).

[53] E.-M. Laine, H.-P. Breuer, and J. Piilo, Sci. Rep. **4**, 4620 (2014).

[54] L. E. Ballentine, *Quantum Mechanics* (World Scientific, 2014), 2nd ed.

[55] T. Heinosaari and M. Ziman, *The Mathematical Language of Quantum Theory: From Uncertainty to Entanglement* (Cambridge University Press, 2011).

[56] P. Busch, M. Grabowski, and P. J. Lahti, *Operational Quantum Physics* (Springer Berlin Heidelberg, 1995).

[57] K. Kraus, A. Böhm, J. D. Dollard, and W. H. Wootters, eds., *States, Effects, and Operations Fundamental Notions of Quantum Theory* (Springer Berlin Heidelberg, 1983).

[58] F. Shibata, Y. Takahashi, and N. Hashitsume, J. Stat. Phys. **17**, 171 (1977).

[59] V. Gorini, A. Kossakowski, and E. C. G. Sudarshan, J. Math. Phys **17**, 821 (1976).

[60] G. Lindblad, Commun. Math. Phys **48**, 119 (1976).

[61] J. Lankinen, H. Lyyra, B. Sokolov, J. Teittinen, B. Ziaei, and S. Maniscalco, Phys. Rev. A **93**, 052103 (2016).

[62] K. Siudzińska and D. Chruściński, arXiv e-prints arXiv:2006.02793 (2020).

[63] M. J. W. Hall, J. D. Cresser, L. Li, and E. Andersson, Phys. Rev. A **89**, 042120 (2014).

[64] M. M. Wolf and J. I. Cirac, Commun. Math. Phys **279**, 147 (2008).

[65] A. Rivas, S. F. Huelga, and M. B. Plenio, Phys. Rev. Lett. **105**, 050403 (2010).

[66] H.-P. Breuer, E.-M. Laine, and J. Piilo, Phys. Rev. Lett. **103**, 210401 (2009).

[67] S. Lorenzo, F. Plastina, and M. Paternostro, Phys. Rev. A **88**, 020102 (2013).

[68] B. Bylicka, D. Chruściński, and S. Maniscalco, Sci. Rep. **4**, 5720 (2014).

[69] D. Chruściński and S. Maniscalco, Phys. Rev. Lett. **112**, 120404 (2014).

[70] T. Baumgratz, M. Cramer, and M. B. Plenio, Phys. Rev. Lett. **113**, 140401 (2014).

[71] C. H. Bennett, H. J. Bernstein, S. Popescu, and B. Schumacher, Phys. Rev. A **53**, 2046 (1996).

[72] W. K. Wootters, Phys. Rev. Lett. **80**, 2245 (1998).

[73] V. Vedral and M. B. Plenio, Phys. Rev. A **57**, 1619 (1998).

[74] R. Horodecki, P. Horodecki, M. Horodecki, and K. Horodecki, Rev. Mod. Phys. **81**, 865 (2009).

[75] M. N. Bera, T. Qureshi, M. A. Siddiqui, and A. K. Pati, Phys. Rev. A **92**, 012118 (2015).

[76] E. Bagan, J. A. Bergou, S. S. Cottrell, and M. Hillery, Phys. Rev. Lett. **116**, 160406 (2016).

[77] M. O. Scully and K. Drühl, Phys. Rev. A **25**, 2208 (1982).

[78] M. O. Scully, B.-G. Englert, and H. Walther, Nature **351**, 111 (1991).

[79] Y.-H. Kim, R. Yu, S. P. Kulik, Y. Shih, and M. O. Scully, Phys. Rev. Lett. **84**, 1 (2000).

[80] S. P. Walborn, M. O. Terra Cunha, S. Pádua, and C. H. Monken, Phys. Rev. A **65**, 033818 (2002).

[81] R. Kosloff, J. Chem. Phys **80**, 1625 (1984).

[82] R. Alicki, M. Horodecki, P. Horodecki, and R. Horodecki, Open Syst. Inf. Dyn. **11**, 205 (2004).

[83] J. Neumann, *Mathematical foundations of quantum mechanics* (Princeton University Press, Princeton N.J, 1955).

[84] M. Esposito, K. Lindenberg, and C. V. den Broeck, New J. Phys. **12**, 013013 (2010).

[85] H. Spohn, J. Math. Phys. **19**, 1227 (1978).

[86] J. Roßnagel, O. Abah, F. Schmidt-Kaler, K. Singer, and E. Lutz, Phys. Rev. Lett. **112**, 030602 (2014).

[87] X.-L. Huang, X.-Y. Niu, X.-M. Xiu, and X.-X. Yi, EPJ D **68**, 32 (2014).

[88] X.-L. Wang, Y.-H. Luo, H.-L. Huang, M.-C. Chen, Z.-E. Su, C. Liu, C. Chen, W. Li, Y.-Q. Fang, X. Jiang, et al., Phys. Rev. Lett. **120**, 260502 (2018).

[89] B. Marques, A. A. Matoso, W. M. Pimenta, A. J. Gutiérrez-Esparza, M. F. Santos, and S. Pádua, Sci. Rep. **5**, 16049 (2015).

[90] L. Mancino, M. Sbroscia, I. Gianani, E. Roccia, and M. Barbieri, Phys. Rev. Lett. **118**, 130502 (2017).

[91] Z.-D. Liu, H. Lyyra, Y.-N. Sun, B.-H. Liu, C.-F. Li, G.-C. Guo, S. Maniscalco, and J. Piilo, Nat. Commun. **9**, 3453 (2018).

[92] O. Siltanen, T. Kuusela, and J. Piilo, Phys. Rev. A **102**, 022225 (2020).

[93] M. Krenn, A. Hochrainer, M. Lahiri, and A. Zeilinger, Phys. Rev. Lett. **118**, 080401 (2017).

[94] M. Krenn, X. Gu, and A. Zeilinger, Phys. Rev. Lett. **119**, 240403 (2017).

[95] V. Coffman, J. Kundu, and W. K. Wootters, Phys. Rev. A **61**, 052306 (2000).

[96] F. Verstraete and H. Verschelde, Phys. Rev. Lett. **90**, 097901 (2003).

[97] V. Mukherjee, V. Giovannetti, R. Fazio, S. F. Huelga, T. Calarco, and S. Montangero, New J. Phys. **17**, 063031 (2015).

[98] A. Das and V. Mukherjee, Phys. Rev. Research **2**, 033083 (2020).

[99] O. Abah and M. Paternostro, J. Phys. Commun. **4**, 085016 (2020).

[100] A. Alecce, F. Galve, N. L. Gullo, L. Dell'Anna, F. Plastina, and R. Zambrini, New J. Phys. **17**, 075007 (2015).

[101] K. Funo, N. Lambert, B. Karimi, J. P. Pekola, Y. Masuyama, and F. Nori, Phys. Rev. B **100**, 035407 (2019).

[102] O. Abah and M. Paternostro, Phys. Rev. E **99**, 022110 (2019).

[103] R. Dann, A. Levy, and R. Kosloff, Phys. Rev. A **98**, 052129 (2018).

[104] A. G. Kofman and G. Kurizki, Phys. Rev. Lett. **93**, 130406 (2004).

[105] G. Gordon, N. Erez, and G. Kurizki, J. Phys. B **40**, S75 (2007).

[106] B. Karimi and J. P. Pekola, Phys. Rev. B **94**, 184503 (2016).

UNIVERSITY OF TURKU

Painosalama Oy, Turku, Finland 2020

ISBN 978-951-29-8275-2 (PRINT)
ISBN 978-951-29-8276-9 (PDF)
ISSN 0082-7002 (Print)
ISSN 2343-3175 (Online)